



# NIH Public Access

## Author Manuscript

*J Am Chem Soc.* Author manuscript; available in PMC 2012 May 10.

Published in final edited form as:

*J Am Chem Soc.* 2010 December 8; 132(48): 17157–17173. doi:10.1021/ja105198c.

## Fast Reactivity of Cyclic Nitrone-Calix[4]pyrrole Conjugate with Superoxide Radical Anion: Theoretical and Experimental Studies<sup>1</sup>

Shang-U Kim<sup>†,‡</sup>, Yangping Liu<sup>‡</sup>, Kevin M. Nash<sup>†</sup>, Jay L. Zweier<sup>†</sup>, Antal Rockenbauer<sup>§</sup>, and Frederick A. Villamena<sup>†,‡,\*</sup>

<sup>†</sup> Department of Pharmacology, Davis Heart and Lung Research Institute, College of Medicine, The Ohio State University, Columbus, OH, 43210, USA

<sup>‡</sup> Center for Biomedical EPR Spectroscopy and Imaging, Davis Heart and Lung Research Institute, College of Medicine, The Ohio State University, Columbus, OH, 43210, USA

<sup>§</sup> Chemical Research Center, Institute of Structural Chemistry, H-1025 Budapest, Pusztaszeri 59, Hungary

### Abstract

Nitron spin traps have been employed as probes for the identification of transient radical species in chemical and biological systems using electron paramagnetic resonance (EPR) spectroscopy, and have found pharmacological activity against oxidative stress-mediated diseases. Since superoxide radical anion ( $O_2^{\bullet-}$ ) is a major precursor to most reactive oxygen species and that calix[4]pyrroles have shown to exhibit high affinity to anions, cyclic nitrone conjugate of calix[4]pyrrole (CalixMPO) was designed, synthesized, and characterized. Computational studies at the PCM/B3LYP/6-31+G(d,p)//B3LYP/6-31G(d) suggest a pendant-type linkage between the calix[4]pyrrole and the nitrone to be the most efficient design for spin trapping of  $O_2^{\bullet-}$ , giving exoergic reaction enthalpies ( $\Delta H_{298K,aq}$ ) and free energies ( $\Delta G_{298K,aq}$ ) of -16.9 and -2.1 kcal/mol, respectively. <sup>1</sup>H NMR study revealed solvent-dependent conformational changes in CalixMPO leading to changes in electronic properties of the nitronyl group upon H-bonding with the pyrrole groups as also confirmed by calculations. CalixMPO spin trapping of  $O_2^{\bullet-}$  exhibited distinctive EPR spectra. Kinetic analysis of  $O_2^{\bullet-}$  adduct formation and decay in polar aprotic solvents using UV-vis stopped-flow and EPR method gave larger trapping rate constant for CalixMPO and longer half-life for its  $O_2^{\bullet-}$  adduct compared to the commonly used nitrones. The unusually high reactivity of CalixMPO to  $O_2^{\bullet-}$  was rationalized to be due to the synergy between  $\alpha$ - and electrostatic effects by the calix[4]pyrrole moiety on the  $O_2^{\bullet-}$  and nitrone, respectively. This work demonstrates for the first time the application of an anion receptor for the detection of one the most important radical intermediates in biological and chemical systems (*i.e.*,  $O_2^{\bullet-}$ ).

### 1. Introduction

Superoxide radical anion ( $O_2^{\bullet-}$ ) is produced from one-electron reduction of triplet dioxygen molecule and is an important precursor to some of the highly oxidizing species that are known to exist in chemical and biological systems.<sup>1</sup> Superoxide can be generated through

<sup>1</sup>Presented in part at the Gordon Conference Oxygen Radicals Meeting, February 7–12, 2010, Ventura, CA.

frederick.villamena@osumc.edu.

Supporting Information Available: Additional figures and tables, synthetic procedures, <sup>1</sup>H and <sup>13</sup>C NMR spectra of all compounds, COSY, HRMS, and IR spectra of CalixMPO, tables for thermodynamics parameters and cartesian coordinates, and complete reference for 69. This material is available free of charge via the Internet at <http://pubs.acs.org>.

chemical, photochemical, and enzymatic means. For example,  $O_2^{\bullet-}$  production has been observed via photolysis of water soluble fullerene C60 or quinones.<sup>2</sup> Superoxide is enzymatically produced via stimulation of NADPH oxidases,<sup>3</sup> leakage from the mitochondrial electron transport chain complexes,<sup>4</sup> oxidation of hypoxanthine by xanthine oxidase<sup>5</sup> or uncoupled nitric oxide synthase.<sup>6</sup> In biological systems, the unregulated production of  $O_2^{\bullet-}$  can lead to the formation of highly oxidizing species causing cellular dysfunction through loss of protein function, carbohydrate oxidation, DNA cleavage, lipid peroxidation, and ultimately, are responsible for the development of a variety of diseases such as cardiovascular and neurodegenerative diseases,<sup>7</sup> cancer,<sup>8</sup> inflammation,<sup>9</sup> acute stroke,<sup>10</sup> or ischemia-reperfusion injury.<sup>11</sup>

EPR spin trapping is a commonly used technique for radical detection which involves formation of radical adducts that exhibit distinctive electron paramagnetic resonance (EPR) spectrum. The direct or indirect observations of  $O_2^{\bullet-}/HO_2^{\bullet}$  formation have been achieved by spin trapping using melanosomes,<sup>12</sup> mitochondria,<sup>13</sup> photosynthetic systems,<sup>14</sup> nitric oxide synthase (NOS),<sup>6, 15</sup> endothelial cells,<sup>16</sup> human neutrophils<sup>17, 18</sup> and reperfused heart tissue.<sup>18, 19</sup> Spin trapping has also found a wide range of applications in the fields of fuel cell research,<sup>20</sup> nanotechnology,<sup>21</sup> catalysis,<sup>22</sup> environmental remediation,<sup>23</sup> and photodynamic therapy.<sup>24</sup> In spite of the popularity of the cyclic nitrones, such as, 5,5-dimethyl pyrroline *N*-oxide (DMPO),<sup>25</sup> and 5-diethoxyphosphoryl-5-methyl pyrroline *N*-oxide (DEPMPO),<sup>26</sup> these nitrones suffer from limitations such as slow reactivity to  $O_2^{\bullet-}$  and poor  $O_2^{\bullet-}$  adduct stability.<sup>27</sup>

Almost 4 decades ago<sup>28</sup> since the inception of nitrone spin traps as probes for radical detection, hundreds of new spin traps with improved properties have been synthesized<sup>29</sup> but these spin traps still suffer from major limitations with either poor reactivity to  $O_2^{\bullet-}$ , short adduct half-life, non-specificity to cellular compartments, or they exhibit spectrum that cannot discern one radical adduct from another.<sup>30</sup> Our laboratory uses computational approach for a rational design of spin traps with improved spin trapping properties.<sup>31</sup> By exploiting the nucleophilic nature of  $O_2^{\bullet-}$  addition to nitrones, the electrophilicity of the nitronyl-C (the site of  $O_2^{\bullet-}$  addition) was increased through conjugation with an amide group at the C-5 position. Furthermore, initial H-bond interaction of the amide substituent with  $O_2^{\bullet-}$  enhances its nucleophilicity to the nitrone *via*  $\alpha$ -effect.<sup>32, 33</sup> Kinetic experimental studies showed that the amide substituted nitrone (AMPO) exhibited a rate constant for  $O_2^{\bullet-}$  trapping in DMF-H<sub>2</sub>O of  $k = 135 \text{ M}^{-1}\text{s}^{-1}$  compared to DMPO and DEPMPO of  $k = 2.0$  and  $0.7 \text{ M}^{-1}\text{s}^{-1}$ , respectively, (or in H<sub>2</sub>O, AMPO:  $25 \text{ M}^{-1}\text{s}^{-1}$ ; DMPO: 2.0; DEPMPO:  $4.0 \text{ M}^{-1}\text{s}^{-1}$ ).<sup>31</sup> The H-bond donor rich  $\beta$ -cyclodextrin-nitronate conjugates, CDNMP and C12CDMPO, linked through an amide bond gave  $k_2$ 's of  $221 \text{ M}^{-1}\text{s}^{-1}$  (DMF-H<sub>2</sub>O) and  $72 \text{ M}^{-1}\text{s}^{-1}$  (in H<sub>2</sub>O), respectively.<sup>34, 35</sup> The role of H-bond donors in increasing  $O_2^{\bullet-}$  nucleophilicity was further demonstrated by Winterbourn *et al.*<sup>36</sup> for tyrosyl hydroperoxide formation and was confirmed by our group to be due to  $\alpha$ -effect.<sup>32</sup> Improved  $O_2^{\bullet-}$  adduct stability was also realized using CDNMP through H-bond stabilization of the radical adduct giving a maximum half-life in water of  $t_{1/2} = 30 \text{ min}$  compared to DMPO and DEPMPO of  $t_{1/2} = 1$  and  $14 \text{ min}$ , respectively (see Figure 1 for structures).<sup>34, 35</sup> However, the permethylated CD-DEPMPO gave  $t_{1/2}$  of  $40 \text{ min}$ <sup>37</sup> indicating that factors other than intramolecular H-bonding can affect adduct stability perhaps via van der Waals interaction.

As pioneered by Sessler and co-workers, a family of calixpyrroles have drawn significant attention in the field of molecular recognition for their convenient synthesis, as well as efficient and selective binding properties to anionic and neutral substrates.<sup>38, 39</sup> Calix[4]pyrroles are macrocyclic molecules consisting of pyrrole rings linked *via* the 2- and 5-positions by sp<sup>3</sup>-hybridized carbon atoms. Over the past years, a large number of calixpyrrole derivatives have been synthesized such as the *meso*-alkyl substituted,<sup>40</sup>

halogenated,<sup>41</sup> C-rim modified,<sup>42</sup> photoactive and chromophore-modified,<sup>43</sup> strapped,<sup>44</sup> ditopic,<sup>45</sup> expanded,<sup>46</sup> N-confused,<sup>47</sup> and polyfunctional analogues<sup>48</sup> exhibiting a variety of recognition properties. Due to the ubiquitousness of anions in many systems, calixpyrroles have been employed as ion-selective receptors<sup>43</sup> and anion-selective optical sensors.<sup>49</sup>

Because of the H-bond donating properties of pyrrole-NH, calix[4]pyrrole may exhibit selectivity towards  $O_2^{\bullet-}$ . We therefore hypothesized that calix[4]pyrrole conjugation with spin traps can offer improved spin trapping properties in terms of increased reactivity to  $O_2^{\bullet-}$  and longer  $O_2^{\bullet-}$  adduct half-life. To the best of our knowledge, there has been no reported application of calix[4]pyrrole in spin trapping and for the first time, this work describes the design, synthesis, and physico-chemical characterization of calix[4]pyrrole-nitrone conjugate exhibiting extraordinarily improved  $O_2^{\bullet-}$  trapping properties and stability for  $O_2^{\bullet-}$  adduct formed, as compared to conventional spin traps.

## 2. Results and Discussion

### 2.1. Computational Studies

**2.1.1. Radical Binding to Calix[4]pyrrole**—The thermodynamics of calix[4]pyrrole binding to various anions (*e.g.*, benzoate,  $Br^-$ ,  $Cl^-$ ,  $CN^-$ ) and neutral substrates (*e.g.*, acetone and MeOH) were calculated and compared to that of  $O_2^{\bullet-}$ , and its protonated form,  $HO_2^{\bullet}$ . Table 1 shows the enthalpies ( $\Delta H_{298K,aq}$ ) and free energies ( $\Delta G_{298K,aq}$ ) as well as bond distances for the pyrrole-NH binding to various substrates (represented by X) in water or DMSO. Results indicate that the calix[4]pyrrole complexes with  $O_2^{\bullet-}$  and  $HO_2^{\bullet}$  were the most favorable by 5.5–10.1 kcal/mol and have relatively shorter NH···X bond distances compared to other non-radical substrates (with the exception of calix[4]pyrrole- $Br^-$  complex). By virtue of symmetry,  $O_2^{\bullet-}$  alone gives equivalent charge and spin density distributions between the two oxygen atoms. However, the calix[4]pyrrole- $O_2^{\bullet-}$  complex gave charge distributions of –0.52 e and –0.29 e for the internal and terminal oxygens, respectively, and spin densities were calculated to be 34% (internal O) and 65% (terminal O). As shown in Figure 2, the calix[4]pyrrole- $O_2^{\bullet-}$  complex is characterized by the presence of strong H-bonding (1.84–1.86 Å) between the pyrrole-NH and superoxide-O. The electronic parameters of  $O_2^{\bullet-}$  upon complexation with calix[4]pyrrole are intermediate between the electronic properties of the free  $O_2^{\bullet-}$  (–0.5 e and 50% for charge and spin densities, respectively) and  $HO_2^{\bullet}$  (–0.20 e and 70% for the terminal O, and –0.36 e and 30% for internal O). This difference in the electron distributions between  $O_2^{\bullet-}$  and  $HO_2^{\bullet}$  ( $pK_a$  4.8)<sup>50</sup> translates to higher reactivity of the latter compared to the former with rate constants of  $O_2^{\bullet-}/HO_2^{\bullet}$  addition to DMPO of 2.0, 27.0 and  $\sim 10^3$  M<sup>-1</sup> s<sup>-1</sup> at pH 7.0, 6.2 and 5.0, respectively,<sup>25, 51</sup> consistent with reduction potentials of  $E^\circ = 0.94$  for  $O_2^{\bullet-}$  and 1.06 V for  $HO_2^{\bullet}$ .<sup>52</sup> Therefore, this polarization of  $O_2^{\bullet-}$  upon complexation with calix[4]pyrrole could enhance  $O_2^{\bullet-}$  reactivity with the nitrone similar to our previous observations for the amide substituted nitrones (AMPO)<sup>31</sup> and tryosyl radicals in the presence of H-bond donors.<sup>32</sup>

Figure 2 also shows the optimized structures for calix[4]pyrrole, its radical cation and anion forms, and complexes with various guest species. The calix[4]pyrrole binding to  $HO_2^{\bullet}$  resulted in the disappearance of spin density distributions on the hydroperoxyl-O's and their redistribution on the methylene carbons of the pyrrole groups. Therefore, electron transfer between  $HO_2^{\bullet}$  and calix[4]pyrrole may occur. The calix[4]pyrrole··· $HO_2^{\bullet}$  gave charge densities of –0.68 e (terminal-O) and –0.57 e (internal-O) with O-O bond length of 1.47 Å, and these electronic properties are intermediate to that observed for  $HO_2^-$  and  $HO_2^{\bullet}$  since examination of the charge densities of  $HO_2^-$  showed –0.83 e (terminal-O) and –0.68 e (internal-O) with a O-O bond length of 1.53 Å, while the O-O bond length for  $HO_2^{\bullet}$  is 1.33 Å and charges of –0.20 e (terminal-O) and –0.36 e (internal-O). For comparison, the electronic properties of [calix[4]pyrrole]<sup>•+</sup> and [calix[4]pyrrole]<sup>•-</sup> were also investigated.

Results indicate that charges are slightly more positive on  $\alpha$ -pyrrolic carbons, less negative on  $\beta$ -pyrrolic carbons and higher spin density distribution on all the pyrrole carbon and nitrogen atoms in [calix[4]pyrrole] $^{+}$  compared to calix[4]pyrrole, while in [calix[4]pyrrole] $^{\bullet-}$ , the pyrrole-N is more negative and the spin densities are more localized on the pyrrole-N and the NH protons. The electronic property of calix[4]pyrrole in the optimized calix[4]pyrrole $\cdots$ HO $_2^{\bullet}$  complex is close to that observed for the [calix[4]pyrrole] $^{+}$  further supporting the oxidation of calix[4]pyrrole by HO $_2^{\bullet}$  to form HO $_2^-$  and [calix[4]pyrrole] $^{+}$ .

The binding energies of calix[4]pyrrole with other biologically relevant reactive species such as peroxy nitrite (ONOO $^-$ ), hydroxyl radical (HO $^\bullet$ ) and hydrogen peroxide (H $_2$ O $_2$ ) were also calculated. As shown in Table 1, complex formation of HO $^\bullet$  is the most exoergic ( $\Delta G_{298K,aq} = -21.6$  kcal/mol), followed by those of ONOO $^-$  and H $_2$ O $_2$  with  $\Delta G_{298K,aq}$  of 12.3 and 15.9 kcal/mol, respectively. Similar to that observed for the redox reaction between HO $_2^{\bullet}$  and calix[4]pyrrole, HO $^\bullet$  binding with calix[4]pyrrole resulted in the formation of HO $^-$  and [calix[4]pyrrole] $^{+}$  as evidenced by the electronic properties predicted for the optimized calix[4]pyrrole $\cdots$ HO $^\bullet$ . The binding of ONOO $^-$  and H $_2$ O $_2$  with calix[4]pyrrole did not result in redox reaction and their energetics are similar to those expected for the other anionic and neutral substrates. The difference in the exoergicity of calix[4]pyrrole complex formation with HO $^\bullet$  and HO $_2^{\bullet}$  is due to their respective reduction potentials of 2.31 V and 1.06 V, respectively.<sup>53</sup> The electrochemical properties of *meso*-octamethyl calix[4]pyrrole have been previously<sup>54</sup> studied using cyclic voltammetry in CH $_2$ Cl $_2$ , and benzonitrile, and gave reduction potentials at 0.92 and 0.82 V, respectively, centered at the pyrrole rings. These higher reduction potentials for HO $^\bullet$  and HO $_2^{\bullet}$  compared to calix[4]pyrrole support the tendency of calix[4]pyrrole to be oxidized in solution by HO $^\bullet$  and HO $_2^{\bullet}$  but not by O $2^{\bullet-}$  due perhaps to their comparable reduction potentials (*i.e.*,  $E^\circ = 0.94$  for O $2^{\bullet-}$ ).

Single point calculations with diffuse functions using B3LYP/6-311+G(d,p) level of theory were performed to account for the negative charges of some guest ions and results indicate no significant difference in the thermochemistry compared to the B3LYP/6-31+G(d,p) level of theory. However, significant difference was observed for the Br $^-$  complex formation between the two levels of theory which could be due to its larger size and its more delocalized charge compared to the other anions considered in this study. The effect of counter cation on the thermochemistry of complex formation was also explored. Two positions for the Na $^+$  were considered as shown in Figure S1, that is, the Na $^+$  is adjacent to the O $2^{\bullet-}$  (top) and the other where the Na $^+$  is below the O $2^{\bullet-}$  (bottom). The thermodynamics of complex formation for calix[4]pyrrole $\cdots$ O $2^{\bullet-}$ +Na $^+$  gave significantly higher endoergic energies compared to the formation of calix[4]pyrrole $\cdots$ O $2^{\bullet-}$  in which the top and bottom positions for the Na $^+$  gave  $\Delta G_{298K,aq}$ 's of 18.2 and 29.7 kcal/mol, respectively, compared to 9.2 kcal/mol in the absence of Na $^+$ . This indicates that formation of calix[4]pyrrole $\cdots$ O $2^{\bullet-}$  + Na $^+$  complex is not favorable, although Gale and co-workers<sup>55</sup> have determined that in the solid state, the anion complexes are in close proximity with their counter cation. Moreover, inclusion of the counter cation leads to a more accurate modeling of NMR spectroscopic data from DFT calculations.<sup>56</sup>

In this work, although the effect of counter cation was not extensively studied for all the complexes, the small difference in the association energy of Na $^+$  ( $\Delta G_{298K,aq} = 3.5$  kcal/mol) with O $2^{\bullet-}$  compared to calix[4]pyrrole (9.2 kcal/mol) indicates that electrostatic interaction can compete with Hbonding interaction. Also, complexation of O $2^{\bullet-}$  to Na $^+$  only resulted in small perturbation of the electron distribution on the two oxygen atoms with charge distributions of -0.56 e and -0.43 e for the internal and terminal oxygens, respectively, and spin densities of 46% (internal O) and 54% (terminal O) (Figure S1). This small change in electron distribution on O $2^{\bullet-}$  with Na $^+$  compared to its complexation with calix[4]pyrrole

suggest that reactivity of  $\text{O}_2^{\bullet-}$  to nitrone will be more influenced by H-bonding interaction with calix[4]pyrrole than electrostatic effect with  $\text{Na}^+$ . Although the thermodynamics of calix[4]pyrrole $\cdots\text{O}_2^{\bullet-}+\text{Na}^+$  formation is highly endoergic, the step-wise mechanism for its formation provides better insight into the possible mode of calix[4]pyrrole $\cdots\text{O}_2^{\bullet-}+\text{Na}^+$  complex formation in solution. The  $\Delta G_{298\text{K},\text{aq}}$  for the initial binding of  $\text{O}_2^{\bullet-}$  to calix[4]pyrrole is 9.2 kcal/mol which is similar or less endoergic compared to the top or bottom addition of  $\text{Na}^+$  to calix[4]pyrrole $\cdots\text{O}_2^{\bullet-}$  (see Figure 3). Therefore, the initial binding of  $\text{O}_2^{\bullet-}$  to calix[4]pyrrole and subsequent addition of the counter cation to the calix[4]pyrrole $\cdots\text{O}_2^{\bullet-}$  complex is the most plausible mechanism and justifies our consideration of only the anion binding for comparing the various enthalpies and free energies of anion binding to calix[4]pyrrole as shown in Table 1.

**2.1.2. Design of Calix[4]pyrrole-Nitronate Conjugate**—Computational studies at the PCM(water)/B3LYP/6-31+G(d,p)//B3LYP/6-31G(d) level of theory were also performed to explore the optimal design that incorporates both the calix[4]pyrrole and nitronate in one molecule. Figure 4 shows three possible spin trap designs where a nitronate and calix[4]pyrrole are coupled via an ester linkage (CalixMPO); two methyl groups were substituted for a pyrrolidine ring to form a spiro compound (**8**); and where one of the pyrrole rings was substituted with nitronate pyrrolidine ring (**9**). (The ester linkage was chosen to fully understand the effect of calix[4]pyrrole moiety on the spin trapping properties of the conjugate since the amide linker group was previously found to exhibit H-bonding properties that can facilitate  $\text{O}_2^{\bullet-}$  addition to nitronates.) Table 2 and Figure 4 shows the thermodynamics of  $\text{O}_2^{\bullet-}$  addition to CalixMPO, **8**, and **9**, and the CalixMPO- $\text{O}_2^{\bullet-}$  adduct gave the lowest free energy of reaction ( $\Delta G_{298\text{K},\text{aq}}$ ) of -2.1 kcal/mol compared to the endoergic reaction free energies calculated for compounds **8** and **9** of 26.7 and 31.1 kcal/mol, respectively. Moreover, the addition of  $\text{HO}_2^{\bullet}$  to CalixMPO is the most favorable with  $\Delta G_{298\text{K},\text{aq}}$  of -5.9 kcal/mol compared to **8** and **9** with  $\Delta G_{298\text{K},\text{aq}}$  of -3.0 and 11.2 kcal/mol, respectively. The favorable energetics for CalixMPO- $\text{O}_2^{\bullet-}$  and CalixMPO- $\text{O}_2^{\bullet}\text{H}$  adduct formations are also reflected in the shorter nitronyl C $\cdots\text{O}_2^{\bullet-}$  bond length by 0.06–0.13 Å, but slightly shorter nitronyl C $\cdots\text{O}_2^{\bullet}\text{H}$  bond length by 0.01–0.02 Å compared to the spin adducts of **8** and **9**. The endoergic free energies of addition of  $\text{O}_2^{\bullet-}$  and  $\text{HO}_2^{\bullet}$  to **8** and **9** could be due to steric hindrance, and therefore, the pendant-type CalixMPO is the best candidate for synthesis. Previous studies also showed polymers containing pendant calixpyrrole subunit exhibiting high affinity towards “hard” potassium salts, thus overcoming the low affinities of calixpyrroles to anions in organic media.<sup>57</sup>

### 2.1.3. Thermodynamics and Kinetics of $\text{O}_2^{\bullet-}$ Addition to CalixMPO

#### 2.1.3.1 Effect of Calix[4]pyrrole on the Thermodynamics of $\text{O}_2^{\bullet-}$ Addition to Nitronates:

The mechanism of  $\text{O}_2^{\bullet-}$  adduct formation at neutral pH proceeds via the rate limiting nucleophilic addition of  $\text{O}_2^{\bullet-}$  to the nitronate to form the aminoxy-O $_2^{\bullet-}$  adduct, which is then followed by protonation to form the aminoxy-O $_2^{\bullet}\text{H}$  adduct ( $\text{p}K_a \sim 15.0$ ).<sup>58</sup> From here onwards, the reference to the formation of  $\text{O}_2^{\bullet-}$  adducts assumes subsequent protonation in solution to form  $\text{HO}_2^{\bullet}$  adducts (see Equation 1) in protic medium, and therefore, the  $\text{O}_2^{\bullet-}$  and  $\text{HO}_2^{\bullet}$  adducts are used interchangeably.

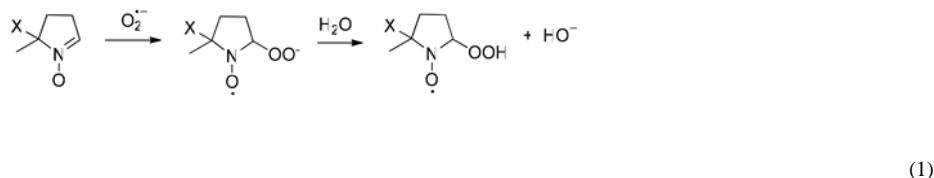


Figure 5 shows the lowest energy conformations for calix[4]pyrrole- $\cdots$ DMPO complex and CalixMPO, and their respective  $O_2^{\bullet-}$  and  $HO_2^{\bullet}$  adducts. A cone-like conformation was exhibited by the unprotonated  $O_2^{\bullet-}$  adduct consistent with the conformation of calix[4]pyrroles with anionic guests (e.g. benzoate,  $Cl^-$ ,  $Br^-$ , and  $CN^-$ ), while 1,3-alternate conformations were found for DMPO- $O_2H$  and CalixMPO- $O_2H$  adducts, which are also consistent with the conformation of calix[4]pyrrole complexes with neutral species such as acetone and MeOH (see Supporting Information for the optimized structures).<sup>39</sup>

To investigate the effect of the calix[4]pyrrole moiety on the favorability of radical addition to nitrones, the enthalpies and free energies of  $O_2^{\bullet-}$  addition to DMPO in the presence of calix[4]pyrrole were calculated and compared to those of CalixMPO (Table 2). Three different scenarios were considered for the formation of calix[4]pyrrole- $\cdots$ DMPO- $O_2^{\bullet-}$ , that is, Mechanism 1 is based on the complex formation from individual calix[4]pyrrole, DMPO and  $O_2^{\bullet-}$ ; Mechanism 2 involves complexation of the initially formed DMPO- $O_2^{\bullet-}$  with calix[4]pyrrole; and Mechanism 3 includes reaction of the initially formed calix[4]pyrrole- $O_2^{\bullet-}$  with DMPO. The order of increasing favorability for the calix[4]pyrrole- $\cdots$ DMPO- $O_2^{\bullet-}$  formation at the PCM(water)/B3LYP/6-31+G(d,p)//B3LYP/6-31G(d) level of theory are  $\Delta G_{298K,aq}^{\circ}$  (in kcal/mol): Mechanism 1 (15.6) < Mechanism 3 (6.4) < Mechanism 2 (3.0), which indicates that a prior reaction of  $O_2^{\bullet-}$  with DMPO or its complexation with calix[4]pyrrole are more favored.

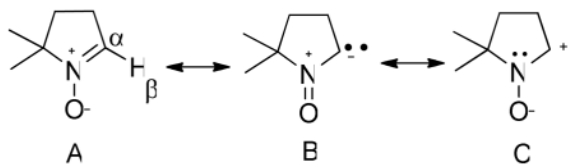
Competition experiments were performed for the spin trapping of  $O_2^{\bullet-}$  using DMPO and increasing concentrations of calix[4]pyrrole. In this experiment, solutions containing various molar ratios of DMPO and calix[4]pyrrole were prepared followed by addition of  $O_2^{\bullet-}$  to these solutions. As monitored by EPR (see Figure S2a), there is a significant decrease in the intensity of DMPO- $O_2^{\bullet-}$  suggesting that calix[4]pyrrole can compete with DMPO for binding with the  $O_2^{\bullet-}$ . Furthermore, the decrease in the signal intensity for DMPO- $O_2^{\bullet-}$  observed in the presence of excess calix[4]pyrrole indicates that the  $O_2^{\bullet-}$  is forming a complex with calix[4]pyrrole resulting in fast dismutation of  $O_2^{\bullet-}$  similar to that observed at slightly acidic pH. Also, in spite of the  $\alpha$ -effect caused by calix[4]pyrrole on the  $O_2^{\bullet-}$ , addition of DMPO to calix[4]pyrrole- $O_2^{\bullet-}$  only results in significantly lower EPR intensity for the  $O_2^{\bullet-}$  adduct formed probably due to the fast dismutation of  $O_2^{\bullet-}$  caused by its polarization upon complexation (see Figure S2b).

The direct addition of  $O_2^{\bullet-}$  to CalixMPO gave preference to the formation of *cis*-adduct ( $\Delta G_{298K,aq}^{\circ} = -2.1$  kcal/mol) than that of *trans*-adduct ( $\Delta G_{298K,aq}^{\circ} = 5.2$  kcal/mol) by *ca.* 7 kcal/mol. Moreover, the formation of  $O_2^{\bullet-}$  adduct of CalixMPO in aqueous phase is most preferred compared to DMPO (11.9), EMPO (9.7), and AMPO (6.1) as previously calculated (see Table S1).<sup>31</sup> These results indicate that the calix[4]pyrrole group and its conjugation to the nitrone plays an important role in the favorability of  $O_2^{\bullet-}$  addition. The effect of  $Na^+$  counter cation on the thermodynamics of CalixMPO- $O_2^{\bullet-}$  formation was also investigated. Similar to that observed for the addition of  $O_2^{\bullet-}$  to calix[4]pyrrole, the initial addition of  $O_2^{\bullet-}$  to CalixMPO is exoergic (-2.1 kcal/mol) compared to the subsequent endoergic addition of  $Na^+$  to the CalixMPO- $O_2^{\bullet-}$  of 21.9 kcal/mol (see Figure 3).

Figure S3 shows the correlations between the charge densities on the nitronyl-C of the various spin traps and the free energies of  $O_2^{\bullet-}$  adduct formation at PCM/B3LYP/6-31+G(d,p) level. The high positive charge density on the nitronyl-C of AMPO compared to other nitrones played an important role on the high rate constant observed for the nucleophilic  $O_2^{\bullet-}$  addition to AMPO. However, the calculated charge density for the nitronyl-C of CalixMPO at the same level of theory is 0.051 e which is only slightly lower compared to AMPO of 0.060 e, indicating that electrostatic effect is not the major factor for the high reactivity of CalixMPO towards  $O_2^{\bullet-}$ , and that this could be due mostly to the  $\alpha$ -

effect caused by the calix[4]pyrrole group on the  $\text{O}_2^{\bullet-}$ . Moreover, the complexation of DMPO to calix[4]pyrrole showed an increase in the charge density on the nitronyl-C of DMPO from 0.02 e to 0.06 e. This effect of calix[4]pyrrole group on the electrophilicity of the nitronyl-C of EMPO will be further discussed under NMR studies in the succeeding section.

To further show the effect calix[4]pyrrole group on the charge density of nitronyl-C, the charge densities were compared in the presence and absence of nitrone and calix[4]pyrrole interaction. In the presence of nitrone- $\text{NO}^{\bullet\bullet}\text{HN}$ -calix[4]pyrrole interaction (in which the nitrone group sits on the annulus of the calix[4]pyrrole), the calculated charge density was found to be 0.051 e, while in the absence of this interaction (see Figure S4), lower charge density of 0.035 e was observed which is closer to that observed for EMPO of 0.040 e. This increase in charge density on the C-2 of the nitrone is due to the increased contribution of the resonance form C during nitrone- $\text{NO}^{\bullet\bullet}\text{HN}$ -calix[4]pyrrole H-bond formation.



Since CalixMPO has an ester linker group and is not conjugated by an amide bond that would allow facilitation of  $\text{O}_2^{\bullet-}$  addition to the nitrone through the amide-NH, the presence of pyrrole-NH in CalixMPO and the proximity of the calix[4]pyrrole ring to the nitrone could play a major role in the facilitation of  $\text{O}_2^{\bullet-}$  addition to the nitrone group via electrostatics and H-bonding.

### **2.1.3.2 Effect of Calix[4]pyrrole on the Energy Barrier of $\text{O}_2^{\bullet-}$ Addition to Nitrones:**

The energy barrier for the addition of calix[4]pyrrole- $\text{O}_2^{\bullet-}$  to DMPO was calculated to be  $\Delta G_{298\text{K},\text{aq}}^{\ddagger} = 25.7 \text{ kcal/mol}$  (Table 3), and this value is similar to that observed for the formation of  $[\text{DMPO-O}_2^{\bullet-}]^{\ddagger}$  (or close in the case of  $[\text{EMPO-O}_2^{\bullet-}]^{\ddagger}$  with  $\Delta G_{298\text{K},\text{aq}}^{\ddagger}$  of 21.1 kcal/mol) as previously calculated (Table S1).<sup>31</sup> Although polarization of the electronic distribution in  $\text{O}_2^{\bullet-}$  upon complexation with calix[4]pyrrole has been observed as discussed above under the **Section 2.1.1**, the energy barrier for the calix[4]pyrrole- $\text{O}_2^{\bullet-}$  addition to DMPO was not lowered indicating that the proximity of the nitrone to the polarized  $\text{O}_2^{\bullet-}$  is again necessary for facile addition of  $\text{O}_2^{\bullet-}$  to the nitrone. Table 3 also shows the energy barrier for CalixMPO- $\text{O}_2^{\bullet-}$  adduct formation with  $\Delta G_{298\text{K},\text{aq}}^{\ddagger} = 17.5 \text{ kcal/mol}$  which is comparable to that previously<sup>31</sup> calculated for AMPO with  $\Delta G_{298\text{K},\text{aq}}^{\ddagger} = 17.4 \text{ kcal/mol}$ . Although the substituent directly attached to CalixMPO is an ester group, the energy barrier observed for CalixMPO is lower compared to that of EMPO but comparable to AMPO which bears an amide substituent. However, examination of the  $[\text{CalixMPO-O}_2^{\bullet-}]^{\ddagger}$  structure revealed that the  $\text{O}_2^{\bullet-}$  exhibits strong H-bond interaction with the four pyrrole-NH's prior to the C-O bond formation to form the adduct. This observation is similar to that observed for the  $[\text{AMPO-O}_2^{\bullet-}]^{\ddagger}$  structure in which the low energy barrier calculated for  $\text{O}_2^{\bullet-}$  addition to AMPO was previously rationalized to be due to the strong H-bonding interaction between amide-NH and  $\text{O}_2^{\bullet-}$  in the TS.

To further confirm the initial mechanism of  $\text{O}_2^{\bullet-}$  addition to CalixMPO, the most preferred CalixMPO conformation was investigated. The most preferred CalixMPO conformation is when the nitrone moiety is away from calix[4]pyrrole group denoted as CalixMPO-180° as shown in Figure S4. The relative free energy of CalixMPO-180° is lower than those of CalixMPO-90° and CalixMPO (**1**) by 0.9 and 3.6 kcal/mol, respectively, which is rationalized to be due to the minimization of steric hinderance. On the other hand, folded

CalixMPO-*cis*-O<sub>2</sub><sup>•-</sup> adduct ( $\Delta G_{298K,\text{rxn}} = -2.1$  kcal/mol) is the most favorable spin adduct conformation, compared to the O<sub>2</sub><sup>•-</sup> adducts of CalixMPO-180° (15.1 kcal/mol) and CalixMPO-90° (11.7 kcal/mol). Since the  $\Delta G_{298K,\text{rxn}}$  of O<sub>2</sub><sup>•-</sup> complexation with calix[4]pyrrole is around 9.2 kcal/mol and that the O<sub>2</sub><sup>•-</sup> addition to the nitrone moiety of the CalixMPO-180° to give CalixMPO-*cis*-O<sub>2</sub><sup>•-</sup> gave  $\Delta G_{298K,\text{rxn}} = 18.3$  kcal/mol, it can be expected that the initial addition to the calix[4]pyrrole can occur. These results support the mechanism in which O<sub>2</sub><sup>•-</sup> adds to the calix[4]pyrrole group of CalixMPO-180° and then the calix[4]pyrrole-O<sub>2</sub><sup>•-</sup> complex facilitate addition to the nitrone group to give the preferred folded CalixMPO-*cis*-O<sub>2</sub><sup>•-</sup> adduct as stabilized via intramolecular H-bonding interaction through the pyrrole-NH's.

The “anchoring” of O<sub>2</sub><sup>•-</sup> to the amide-NH results in the polarization of the O<sub>2</sub><sup>•-</sup> electron distribution known as  $\alpha$ -effect.<sup>31</sup> Although the energy barriers for the formation of [CalixMPO-O<sub>2</sub><sup>•-</sup>]<sup>‡</sup> and [AMPO-O<sub>2</sub><sup>•-</sup>]<sup>‡</sup> are almost similar, the calculated  $\Delta G_{298K,\text{aq}}$  for the formation of CalixMPO-O<sub>2</sub><sup>•-</sup> and AMPO-O<sub>2</sub><sup>•-</sup> are significantly different, in which the former is exoergic (-2.1 kcal/mol) than the latter (6.1 kcal/mol) indicating that O<sub>2</sub><sup>•-</sup> addition to CalixMPO can be both thermodynamically and kinetically favorable compared to other nitrones considered in this study. Based on the similarity in the  $\Delta G^\ddagger_{298K,\text{aq}}$  for [CalixMPO-O<sub>2</sub><sup>•-</sup>]<sup>‡</sup> and [AMPO-O<sub>2</sub><sup>•-</sup>]<sup>‡</sup>, and the more stable final state for CalixMPO-O<sub>2</sub><sup>•-</sup> compared to AMPO-O<sub>2</sub><sup>•-</sup>, the potential energy surface for the CalixMPO-O<sub>2</sub><sup>•-</sup> formation can be visualized to have a reactant-like or early transition state surface. This study also further shows the necessity of having the H-bond donor at close proximity to the nitrone moiety that can obviously be achieved via conjugation thus allowing a concerted mechanism by which the O<sub>2</sub><sup>•-</sup> can undergo H-bond interaction resulting into its polarization and eventual facile addition to the nitrone.

**2.1.4. Thermodynamics of HO<sub>2</sub><sup>•</sup> Addition to CalixMPO**—Allouch *et al.*<sup>51</sup> showed that O<sub>2</sub><sup>•-</sup> reactivity to nitrones in acidic pH was enhanced due to the formation of HO<sub>2</sub><sup>•</sup>. We have previously proposed that in acidic pH, the direct addition of HO<sub>2</sub><sup>•</sup> to the nitrone was the major mechanism for HO<sub>2</sub><sup>•</sup> adduct formation.<sup>58</sup> The thermodynamics of HO<sub>2</sub><sup>•</sup> addition to DMPO in the presence of calix[4]pyrrole, and to CalixMPO were also investigated. As shown in Table 2, prior complexation of the HO<sub>2</sub><sup>•</sup> to calix[4]pyrrole is the most preferred (6.6 kcal/mol), but unlike in O<sub>2</sub><sup>•-</sup>, the complexation of DMPO-O<sub>2</sub>H is the least preferred (20.6 kcal/mol). Nevertheless, HO<sub>2</sub><sup>•</sup> addition to CalixMPO is exoergic, with the *trans* addition being more favored than *cis* addition with  $\Delta G_{298K,\text{aq}} = -5.9$  and -1.9 kcal/mol, respectively, contrary to the preferred mode of O<sub>2</sub><sup>•-</sup> addition (*i.e.*, *cis*) which further supports our hypothesis that prior complexation of O<sub>2</sub><sup>•-</sup> to the calix[4]pyrrole moiety occurs for the facile O<sub>2</sub><sup>•-</sup> addition to nitrone. The previously calculated  $\Delta G_{298K,\text{aq}}$  of HO<sub>2</sub><sup>•</sup> addition to nitrone at the same level of theory are (in kcal/mol): PBN (-0.9),<sup>59</sup> AMPO (-1.6),<sup>60</sup> DEPMPO (-4.8),<sup>60</sup> EMPO (-6.2)<sup>60</sup> and DMPO (-4.6),<sup>60</sup> and these energies are comparable to the formation of CalixMPO-O<sub>2</sub>H adduct with an exoergic  $\Delta G_{298K,\text{aq}}$  of -5.9 kcal/mol indicating that calix[4]pyrrole group has no significant effect on the reactivity of HO<sub>2</sub><sup>•</sup>. This further supports our initial findings that the nature of HO<sub>2</sub><sup>•</sup> addition to nitrones is mostly electrophilic in nature contrary to the nucleophilic nature of O<sub>2</sub><sup>•-</sup> addition to nitrones.<sup>31, 60</sup>

## 2.2 Synthesis and Characterization

**2.2.1 Synthesis of CalixMPO**—The synthesis of CalixMPO (**1**) is shown in Scheme 1. The calix[4]pyrrole ethyl ester (**6**) was first synthesized in one step from pyrrole, ethyl pyruvate, and acetone in the presence of methanesulfonic acid in methanol.<sup>40</sup> Subsequently, the ester (**6**) was reduced by NaBH<sub>4</sub> in EtOH/H<sub>2</sub>O to the mono-hydroxy calix[4]pyrrole (**5**) in 75%.<sup>61</sup> Finally, the efficient coupling between CMPO (**2**)<sup>62</sup> and the alcohol (**5**) using EDC, HOBt, and catalytic amount of Et<sub>3</sub>N in CH<sub>2</sub>Cl<sub>2</sub> or CH<sub>3</sub>CN resulted in the nitrone

conjugate of calix[4]pyrrole (**1**) with a yield of 16%, which was well characterized by  $^1\text{H}$ ,  $^{13}\text{C}$ , and  $^1\text{H}$ - $^1\text{H}$  COSY NMR, IR and HRMS spectroscopies. Attempts to use other polar aprotic solvents (*e.g.*, DMF and DMSO) were unsuccessful. In addition, the yield was not improved by extending the reaction time to 48 h or by heating to 40–45 °C.

### 2.2.2. NMR Studies

**2.2.2.1. Solvent Dependence of CalixMPO Conformation:** Table S2 shows the  $^1\text{H}$  chemical shifts for compounds **1** through **7**. The H-2 chemical shift for CalixMPO was found to be 5.42 ppm in  $\text{CDCl}_3$  which is unusually upfield compared to EMPO at 6.87 ppm in  $\text{CDCl}_3$ .  $^1\text{H}$ - $^1\text{H}$  COSY spectra shows that H-2 for CalixMPO correlates with two methylene peaks (H-3) at 2.14 and 2.24 ppm and long range coupling with the methyl H-6 peak at 1.67 ppm (Figure 6), but no correlation between the H-2 and the protons from the calix[4]pyrrole ring was observed (see Supporting Information for full spectrum of COSY). On the other hand, the H-2 of CalixMPO in  $\text{DMSO}-d_6$  was observed at 6.90 ppm, which is very close to the H-2 chemical shift of EMPO (6.99 ppm) in the same solvent (see Supporting Information). These results indicate that the H-2 chemical shift of CalixMPO is solvent-dependent, presumably due to the difference in conformation of calix[4]pyrrole moiety in DMSO and  $\text{CHCl}_3$  resulting to varying degrees of shielding by the pyrrole groups.

To further investigate the solvent-dependence of the chemical shift of the H-2 caused by the calix[4]pyrrole, the chemical shift of the H-2 in  $\text{DMSO}-d_6$  was monitored as a function of increasing amounts of  $\text{CDCl}_3$  (Figure 7). Results show an upfield shift for H-2 suggesting that this proton becomes more shielded in  $\text{CDCl}_3$ . The more downfield chemical shift of the H-2 in  $\text{DMSO}-d_6$  (6.90 ppm) compared in  $\text{CDCl}_3$  (5.42 ppm) is due to the less shielding of the nitrone group by the  $\pi$ -systems of the pyrrole rings as they assume a cone-type conformation in  $\text{DMSO}-d_6$ . The cone-type conformation in  $\text{DMSO}-d_6$  is supported by  $^1\text{H}$  NMR studies as discussed below. However, the 1,3-alternate conformation of the calix[4]pyrrole group in  $\text{CDCl}_3$  causes higher interaction of the pi-systems with the nitrone moiety. This conformation is also supported by the observed  $^1\text{H}$  NMR shifts in  $\text{CDCl}_3$  which will be presented in the succeeding section. Computational studies<sup>63</sup> revealed higher probability of cone conformation in DMSO with dielectric constant ( $\epsilon$ ) of 46.7 than in  $\text{CH}_2\text{Cl}_2$  ( $\epsilon = 9.1$ ) and since  $\text{CHCl}_3$  has a dielectric constant of 4.8 which is closer to  $\text{CH}_2\text{Cl}_2$ , it can be expected that the cone conformation in  $\text{CHCl}_3$  is not preferable.

The chemical shifts of pyrrole-NH for each of the calix[4]pyrrole-containing compounds (*i.e.*, CalixMPO, **5**, **6**, and **7**) were also investigated (see Figure S5). In  $\text{CDCl}_3$ , **5** gave two non-equivalent pyrrole-NH's as evidenced by two  $^1\text{H}$ -NMR peaks at 7.05 and 7.54 ppm, and the same  $^1\text{H}$  NMR profile was observed for **6** with peaks at 7.08 and 7.44 ppm. However, **7** only gave one peak at 6.98 ppm indicating the presence of 4 equivalent pyrrole-NH's by virtue of symmetry. However, the four pyrrole NH's of CalixMPO in  $\text{CDCl}_3$ , are non-equivalent with peaks at 7.36, 7.55, 9.48, and 9.60 ppm, while in  $\text{DMSO}-d_6$ , the four pyrrole-NH's gave chemical shift values that are close to one another, that is, 9.24, 9.34, 9.46, and 9.51 ppm, due perhaps to the preferred cone-like conformation in this solvent. The difference in  $^1\text{H}$  NMR spectral profile for CalixMPO in  $\text{DMSO}-d_6$  and in  $\text{CDCl}_3$  further supports the cone-type and 1,3-alternate conformations in these solvents, respectively.

**2.2.2.2. Effect of Calix[4]pyrrole on C-2 Charge Density:** Computational studies show the effect of calix[4]pyrrole moiety on the charge density of the nitronyl-C. To further confirm these theoretical results,  $^1\text{H}$  and  $^{13}\text{C}$  NMR of EMPO in  $\text{CDCl}_3$  solutions containing 0.5, 1.0, and 2.0 equivalents of *meso*-octamethyl calix[4]pyrrole were obtained. Figure 8 shows that increasing equivalence of calix[4]pyrrole gives a slight downfield shift for H-2 which is characteristic of proton deshielding. Similarly, the  $^{13}\text{C}$ -NMR chemical shift of C-2 also

exhibited a downfield shift (Table S3) with increasing equivalence of calix[4]pyrrole. These NMR results can be rationalized to be due to the intermolecular H-bonding between pyrrole-NH and *N*-oxide-O resulting in lowered electron density distribution on C-2. A downfield shift in  $^1\text{H}$  and  $^{13}\text{C}$  NMR resonances was also observed for H-2 and C-2 in DMPO as a function of increasing acidity which was accounted to the protonation of nitronyl-O resulting in larger contribution of positive charge on the nitronyl-C.<sup>64</sup> This NMR study is consistent with the observations made from the computational studies mentioned above in which the nitrone-NO<sup>··-</sup>HN-calix[4]pyrrole interaction can increase the C-2 charge density.

### 2.3. EPR Spin Trapping

Spin adducts were generated in mixed solvents due to the poor solubility of CalixMPO in aqueous system. EPR spectra were generated (Figure 9) from CalixMPO and using various radical generating systems such as light-riboflavin in PBS with 50% acetonitrile, KO<sub>2</sub> in DMSO with 15% PBS, H<sub>2</sub>O<sub>2</sub> in pyridine with 10% PBS, and H<sub>2</sub>O<sub>2</sub>/FeSO<sub>4</sub> in PBS with 50% ethanol (see Experimental Section for details). All the spectra exhibited dynamic lineshape effect as characterized by a broadened linewidth of the high-field line—characteristic of hindered molecular tumbling due to molecular size and solvent interaction. Figures 9a–9c gave EPR spectra for the major adduct with  $a_{\text{N}}$  and  $a_{\beta-\text{H}}$  ranging from 12.39–12.95 G and 10.31–11.11 G, respectively. These spectra can be assigned to HO<sub>2</sub><sup>·</sup> adducts as confirmed by using DEPMPO as a spin trap (see Figure S6).

Figure 9c shows the EPR spectrum of the HO<sub>2</sub><sup>·</sup> adduct generated from H<sub>2</sub>O<sub>2</sub> in pyridine. The spectrum is relatively clean but broader linewidth and with hyperfine splitting constants (hfsc's) similar to that observed in Figure 9a and 9b. As we discussed previously,<sup>59</sup> the mechanism for HO<sub>2</sub><sup>·</sup> adduct formation can occur via via nucleophilic addition of HO<sub>2</sub><sup>·</sup> to nitrone to yield the hydroxylamine and subsequent oxidation by O<sub>2</sub> to afford the aminoxy adduct through direct HO<sub>2</sub><sup>·</sup> addition to the nitrone but the latter mechanism is more plausible due to the higher p*K*<sub>a</sub> of the conjugate acid of pyridine (5.2) compared to H<sub>2</sub>O<sub>2</sub> (11.2), and that previous chemistry involving H<sub>2</sub>O<sub>2</sub>/pyridine shows formation of quinones and enones from aromatic systems further supporting the radical-mediated reaction. Figure 9d shows the EPR spectrum of the CalixMPO radical adducts generated from H<sub>2</sub>O<sub>2</sub>/FeSO<sub>4</sub> in 50% aqueous ethanolic solution. The spectrum is characteristic of carbon-centered adduct (~80%) originating from α-hydroxyethyl radical (CH<sub>3</sub><sup>·</sup>CHOH) along with smaller proportion of HO<sup>·</sup> adduct (~20%). The simulated spectrum for the CalixMPO-OH revealed hfsc's of  $a_{\text{N}} = 13.38$  G and  $a_{\text{H}} = 10.80$  G which is slightly different from the hfsc's observed for the HO<sub>2</sub><sup>·</sup> adducts where the observed  $a_{\text{N}}$ 's are much lower. The alkyl adducts observed in Figure 9a and 9d gave  $a_{\text{N}} = 14.48$ –14.51 G and  $a_{\text{H}} = 20.27$ –20.70 G. The HO<sup>·</sup> adduct of CalixMPO was generated in PBS with 50% acetonitrile, and gave hfsc's of  $a_{\text{N}} = 13.79$  G and  $a_{\text{H}} = 11.65$  G in which the observed  $a_{\text{N}}$  is also higher compared to those observed for HO<sub>2</sub><sup>·</sup> adducts. By careful simulations, one should be able to distinguish between the CalixMPO-OH and CalixMPO-OOH adducts.

### 2.4. Kinetics Studies

#### 2.4.1 Kinetics of O<sub>2</sub><sup>·-</sup> Adduct Formation

**2.4.1.1. UV-vis Stopped-Flow Kinetics:** Figure 10 shows the EPR spectra of the O<sub>2</sub><sup>·-</sup> adduct of DMPO and CalixMPO using the same experimental conditions. The intensity of CalixMPO-O<sub>2</sub>H adduct was *ca.* 18 times higher than that of DMPO-O<sub>2</sub>H, suggesting that CalixMPO has more efficient O<sub>2</sub><sup>·-</sup> trapping ability compared to DMPO. To determine the rate constant ( $k_2$ ) of CalixMPO trapping of O<sub>2</sub><sup>·-</sup>, stopped-flow competitive kinetics was carried out in DMF according to published procedure<sup>59</sup> in which the growth of the transient absorption at 575 nm from the reaction between O<sub>2</sub><sup>·-</sup> and phenol red (PR) was monitored using UV-vis spectroscopy. The relative rate constants was determined using Equation 2

where  $V$  and  $v$  are the initial rates of the  $\text{O}_2^{\bullet-}$  reaction with PR in the absence and presence of the nitrone, respectively.

$$\frac{V}{v} - 1 = \frac{k_{nitrone}[\text{nitrone}]}{k_{PR}[\text{PR}]} \quad (2)$$

Figure 11 shows the plots of  $V/v - 1$  versus [CalixMPO]/[PR] and gave  $k_{\text{CalixMPO}}/k_{\text{PR}}$  of  $12.04 \pm 1.46$ , while the  $k_{\text{DMPO}}/k_{\text{PR}}$  was found to be  $0.03 \pm 0.00$  indicating that CalixMPO traps  $\text{O}_2^{\bullet-}$  ca. 400 times faster than DMPO in DMF. Using the  $k_2$  determined for DMPO<sup>31</sup> of  $1.7 \text{ M}^{-1}\text{s}^{-1}$ , the  $k_2$  for the CalixMPO can be approximated to be  $\sim 680 \pm 80 \text{ M}^{-1}\text{s}^{-1}$  which is much higher than the previously determined  $k_2$ 's in DMF using the same technique, that is, AMPO ( $135 \text{ M}^{-1}\text{s}^{-1}$ )<sup>31</sup>; EMPO ( $104 \text{ M}^{-1}\text{s}^{-1}$ )<sup>31</sup>; DEPMPO ( $0.7 \text{ M}^{-1}\text{s}^{-1}$ )<sup>31</sup>; PBN ( $0.1\text{--}0.8 \text{ M}^{-1}\text{s}^{-1}$ )<sup>59</sup>; and C12CDMPO ( $221 \text{ M}^{-1}\text{s}^{-1}$ )<sup>34</sup> (see Figure 1 for structures) indicating that CalixMPO exhibited the highest rate constant for  $\text{O}_2^{\bullet-}$  trapping in DMF observed thus far for a cyclic nitrone using the same experimental conditions. To investigate the contribution of the calix[4]pyrrole moiety on the observed rate constant for the trapping of  $\text{O}_2^{\bullet-}$  by CalixMPO, calix[4]pyrrole ethyl ester (**6**) was used for the competitive stopped-flow kinetic studies and show a relatively high  $k_{\text{Calix-OEt}}/k_{\text{PR}}$  ratio of  $2.0 \pm 0.3 \text{ M}^{-1}\text{s}^{-1}$  which indicates that **6** is ca. 65 times faster than that observed for DMPO. The mechanism for the  $\text{O}_2^{\bullet-}$  reaction with **6** could be mostly due to dismutation perhaps as catalyzed by the polarization of the spin and charge density distributions as shown by our theoretical studies mentioned above. Due to the proximity of the nitrone group to the calix[4]pyrrole moiety, a concerted addition reaction could be a more plausible mechanism in which initial complexation of the  $\text{O}_2^{\bullet-}$  to the calix[4]pyrrole moiety occurs followed by the addition of the electronically polarized  $\text{O}_2^{\bullet-}$  to the nitrone moiety. This mechanism was similar to the one previously proposed<sup>31</sup> for the amide-substituted nitrones, AMPO. Therefore, the presence of calix[4]pyrrole subunit can greatly improve  $\text{O}_2^{\bullet-}$  reactivity to the nitrone.

**2.4.1.2. EPR Stopped-Flow Kinetics:** The trend in rate constants from the UV-vis stopped flow kinetics was further confirmed by another technique using EPR stopped-flow method. Due to the limited solubility of CalixMPO in water where the conventional kinetic methodologies for  $\text{O}_2^{\bullet-}$  radical generation are not possible (e.g., using xanthine-xanthine oxidase or photolysis with riboflavin), a set-up was designed such that the reactants could be injected via syringe directly into the EPR cell to dramatically cut the time from mixing to the initial data acquisition (see Experimental Section). Only in pure DMSO solutions of  $\text{KO}_2$  and nitrones where it was found that it is feasible to observe decent signal formation. The experimental conditions do not allow to follow the build-up of signal formation, thus a crude estimation by using the maximum adduct concentrations was used and can offer an estimation of the ratios of trapping rates. For this purpose the lowest nitrone concentration gives the most relevant information, that is, the competition between the dismutation of primary  $\text{O}_2^{\bullet-}$  formed and the rate of scavenging can determine the maximum concentration. As shown in Figure S7, the smallest nitrone concentration is  $0.5 \text{ mM}$  for CalixMPO, EMPO and AMPO where the signal can be observed, while it is  $1.0 \text{ mM}$  for DEPMPO and DMPO. Moreover, by considering the observed concentrations, we can estimate the ratio of rate constants ( $k_T$ ). As shown in Table 4, CalixMPO is the fastest spin trap for  $\text{O}_2^{\bullet-}$  but its rate constant is only one order of magnitude faster compared to DMPO and DEPMPO. Also, when the decay is very fast, it can also reduce the maximum signal intensity. Therefore,  $k_T$  can be underestimated in these cases. For EMPO, AMPO and CalixMPO, the ratios of concentrations were 1:2:4, which correspond to the ratio of respective rate constants. For DMPO and DEPMPO, the adduct concentrations were the same and while the necessary nitrone concentration needed to give a detectable was twice as much as in the case of

EMPO, AMPO and CalixMPO, the respective rate constants for DMPO and DEPMPO can be approximated to be half than in the case of EMPO. It should be noted that the assumption made in this calculation was that the decay rates were all identical. But since this is obviously not the case, the suggested ratios for the rate constants are rather approximates, but their order can be correct. The trend nevertheless follows that of the UV-vis stopped-flow technique previously employed.

#### **2.4.1.3. Difference in the Magnitudes of Rate Constant Values between UV-vis and EPR Techniques:**

The observed trend in rate constants using the UV-vis technique correlates well with the EPR in which the order of decreasing reactivity to  $O_2^{\bullet-}$  is as follows: CalixMPO > AMPO > EMPO > DEPMPO  $\approx$  DMPO. However, there is significant discrepancy in the magnitudes of rate constants between the two methods and this can be due to the fact that the EPR technique only monitors the rate of formation of the nitrono- $O_2^{\bullet-}$  adduct, while the UV-vis stopped-flow technique monitors the rate of  $O_2^{\bullet-}$  decay that is dependent on the nitrono's concentration. Moreover, since simultaneous spin-adduct formation and decay occurs during spin trapping, the EPR technique could not account for the  $O_2^{\bullet-}$  adducts that decomposed during spin adduct formation while the UV-vis stopped-flow technique accounts for *all* of the reactions which deplete the concentration of  $O_2^{\bullet-}$  and which depend on the nitrono's concentration. Also, solvent effects can significantly affect the rate of adduct formation and adduct stability as discussed. Reaction in pure DMSO using EPR only allows the addition of  $O_2^{\bullet-}$  to the nitrono while the UV-vis technique considers the reaction of the  $HO_2^{\bullet}$  and  $O_2^{\bullet-}$  species due to the presence of water. It has been shown that  $HO_2^{\bullet}$  exhibits higher reactivity with nitrones compared to  $O_2^{\bullet-}$  as we explained above.

#### **2.4.2 Correlation of Experimental and Theoretical Rate Constants—**

The experimental and calculated rate constants as well as the reaction free energies for the  $O_2^{\bullet-}$  adducts formation are presented in Table 4 along with the nitronyl-C charge densities of their respective nitrones. In general, the qualitative trend in the calculated rate constants at the PCM(water or DMSO)/B3LYP/6-31+G(d,p)//B3LYP/6-31G(d) level of theory follows that of the experimental values for the nitrones with the exception of AMPO and CalixMPO where the trend in their experimental rate constants do not correlate well with the calculated values. However, good correlation can be seen with calculated free energies ( $\Delta G_{298K,aq}^{\ddagger}$ ) and experimental rate constants for  $O_2^{\bullet-}$  adduct formation in aqueous system and in DMSO with CalixMPO giving the only exoergic  $\Delta G_{298K,aq}^{\ddagger}$  for  $O_2^{\bullet-}$  adduct formation compared to other spin traps. This result suggest future consideration of both the  $\Delta G_{298K,aq}^{\ddagger}$  and  $\Delta G_{rxn}^{\ddagger}$  in predicting more accurate experimental rate constants.

It is important to note that the C-2 charge densities are higher for CalixMPO and AMPO compared to other nitrones but AMPO gave a slightly higher charge density (0.060 e) than CalixMPO (0.051 e) indicating that electrostatic effect on the nucleophilic addition of  $O_2^{\bullet-}$  to CalixMPO is not the main factor for the high rate constant experimentally observed for CalixMPO. Moreover, the lower C-2 charge density in CalixMPO compared to AMPO is due to the difference in the nature of the linker group attached to the parent ring. In spite of the same ester group present in both EMPO and CalixMPO, the latter still exhibits slightly higher C-2 charge density than the former (0.040 e) indicating that the calix[4]pyrrole group affects the charge density on the C-2. This effect is further confirmed by the  $^1H$  NMR studies previously discussed in Section 2.2.2.2. in which free calix[4]pyrrole enhances the positivity of the C-2 of EMPO. This through-space mechanism rather than through-bond inductive effect in enhancing C-2 positivity by calix[4]pyrrole group was also demonstrated computationally in which the the C-2 charge density is significantly higher (0.051 e) when the nitrone sits on the annulus of the calix[4]pyrrole group and H-bonded to it compared to when the nitrone group is not-H-bonded giving charge densities of only 0.035–0.038 e (see Figure S4).

**2.4.3 Kinetics of  $O_2^{\bullet-}$  Adduct Decay**—Due to the poor solubility of CalixMPO in water, the decay kinetics was investigated in 85% DMSO-15% PBS by monitoring the decay of the EPR signal as a function of time and was compared to that of DMPO (Figure 11). As shown in Figure 12, CalixMPO $O_2$ H exhibited longer half-life than DMPO and the half-lives were calculated based on first-order decay kinetics as  $24.9 \pm 4.1$  min and  $6.1 \pm 1.8$  min, respectively. In spite of the potential for DMSO to annihilate the intramolecular H-bond interaction leading to short-adduct half-life, the longer half-life observed for CalixMPO- $O_2$ H of  $\sim 25$  min in DMSO compared to that of CDNMPO- $O_2$ H ( $t_{1/2} \sim 6$  min) and C12CDMPO- $O_2$ H ( $t_{1/2} \sim 9$  min) could be due to the preference of the calix[4]pyrrole moiety to forcibly assume a cone-type conformation in DMSO which in turn can stabilize the spin adduct. As shown in Figure 5, the presence of H-bonding of the pyrrole-NH with the two hydroperoxy-O's are evident and are potential factors for the adduct stability.

Our previous studies showed that the spiro-lactonyl nitron (CPCOMPO) containing rigid H-bond acceptor exhibited unstable  $O_2^{\bullet-}$  adduct as evidenced by the relatively fast decay ( $t_{1/2} = 2.4$  min) of its EPR spectra in aqueous solution.<sup>65</sup> Longer first order half-life of the  $O_2^{\bullet-}$  adduct was achieved from  $\beta$ -cyclodextrin-nitron conjugate (CDNMPO) giving a maximum  $t_{1/2}$  of 28 min in aqueous system.<sup>35</sup> This longer half-life for CDNMPO- $O_2$ H was due to the extensive intramolecular H-bonding interaction of the hydroperoxyl moiety with the hydroxyl groups of the cyclodextrin thus stabilizing the adduct. The effect of H-bonding interaction on the stability of the adduct was further confirmed by measuring the half-life of CDNMPO- $O_2$ H in DMSO as well and result shows that the  $t_{1/2}$  was significantly shortened to  $\sim 6$  min due perhaps to the destruction of H-bond interaction in DMSO indicating that intramolecular H-bonding interaction play a major role in adduct stability (see Figure 1 for structures). Aside from the role of intramolecular H-bonding interaction on adduct stability, it is also important to emphasize the better protection of calix[4]pyrrole on the adduct against attack of the primary radical,  $O_2^{\bullet-}$ , compared to any other trap. We previously<sup>66</sup> shown the redox reaction of  $O_2^{\bullet-}$  adducts with  $O_2^{\bullet-}$  to form the *N*-olate anion and oxoammonium cation with the formation of the former being just slightly more favored than the later by  $\sim 0.1$  kcal/mol at the PCM/BHandLYP/6-311G(d,p)//B3LYP/6-31G(d) level of theory. The susceptibility of  $O_2^{\bullet-}$  adducts to reduction by  $O_2^{\bullet-}$  correlates better with their experimental half-lives than their unimolecular decomposition.<sup>67</sup>

The decay kinetics for various nitrones using the EPR stopped-flow technique in pure DMSO was also determined. The decay profile is described by a fast initial decay and then followed by slow decay perhaps due to the fast reaction of the primary radical with the adduct and exhaustion of the radical source, respectively. As shown in Table S4, except with CalixMPO, the initial lifetimes of the adducts are very short (*i.e.*, 0.3–1.8 min) at concentration range of 0.5–15 mM. It appears that these adducts are susceptible to primary radical attack. The CalixMPO adduct seems to be the most protected against the attack of primary radicals with an initial decay time of 5–15 min over a concentration range 0.5–10 mM. One interesting observation about the  $O_2^{\bullet-}$  adduct decay in pure DMSO is the formation of secondary radical adducts (see Figure S8) from the decomposition of the primary adduct. In 100% DMSO, the primary adduct ( $g = 2.0058$ ,  $a_N = 13.2$ ,  $a_H = 11.4$ ,  $a_{H'} = 1.4$ ) decomposes and new radicals species are formed right at the beginning as opposed to in 85% DMSO-15% H<sub>2</sub>O, the primary radical ( $g = 2.0057$ ,  $a_N = 12.8$ ,  $a_H = 10.7$ ,  $a_{H'} = 1.0$ ) is rather stable, with only 4% of other radicals (probably a HO<sup>•</sup> adduct with  $g = 2.0057$ ,  $a_N = 14.4$ ,  $a_H = 12.8$ ,  $a_{H'} = 0.6$ ) present.

### 3. Experimental Section

#### Computational Method

All calculations were performed at the Ohio Supercomputer Center. For each structures, initial conformational search was performed using Spartan 04 at MMFF level. Density functional theory (DFT)<sup>68</sup> was applied to determine the optimized geometry, vibrational frequency, and single-point energy of all stationary points using Gaussian 03<sup>69</sup>. Single point energies were obtained at the B3LYP/6-31+G(d,p) level based on the optimized B3LYP/6-31G(p) geometries. Spin adduct structures were chosen based on the most stable conformer/configurations in aqueous solution and DMSO *via* polarizable continuum model (PCM) using single-point energy calculations at the B3LYP/6-31+G(d,p) level.<sup>70</sup> A scaling factor of 0.9806<sup>71</sup> was used for the zero-point vibrational energy (ZPE) correction for the B3LYP geometries. Free energies were obtained from the calculated thermal and entropic corrections at 298K using the unscaled vibrational frequencies. The charge densities were obtained from a natural population analysis (NPA) approach<sup>72</sup> at the single-point PCM/B3LYP/6-31+G(d,p)//B3LYP/6-31G(d) levels. For the minima, spin contamination for the adduct radicals are negligible, *i.e.*,  $0.75 < \langle S^2 \rangle < 0.76$ .

#### EPR Measurements

EPR measurements were carried out on an EPR spectrometer equipped with high sensitivity resonator at room temperature. Unless otherwise indicated, the instrument settings used for general spectral acquisition are: microwave power, 10 mW; modulation amplitude, 1 G; receiver gain,  $1.0 \times 10^4$  or  $1.0 \times 10^5$ ; scan time 21.5 s; time constant, 42.0 s; sweep width, 120 G. Scans were integrated using the Bruker WINEPR v.2.11b software. All the spin trapping studies were carried out in DMSO or a phosphate buffer (PBS) (10 mM) at pH 7.0 containing 100  $\mu$ M diethylene triamine pentaacetic acid (DTPA). Sample cells used were 50  $\mu$ L glass capillary tubes. The spectrum simulation was carried out by an automatic fitting program.<sup>73</sup>

#### Spin Trapping

- a) **Superoxide radical anion.** i) **KO<sub>2</sub> generating system.** 100 mM CalixMPO solution in DMSO (7.5  $\mu$ L) was diluted with PBS (7.5  $\mu$ L) and DMSO (30  $\mu$ L). Superoxide adduct was generated by adding saturated KO<sub>2</sub> solution in DMSO (5  $\mu$ L) to the resulting CalixMPO solution (45  $\mu$ L). ii) **Light-riboflavin generating system.** 20 mM CalixMPO and 500  $\mu$ M riboflavin in acetonitrile (20  $\mu$ L) was diluted with PBS (25  $\mu$ L) and acetonitrile (5  $\mu$ L). The resulting solution was bubbled with air for 5 min and then was irradiated using visible light.. iii) **H<sub>2</sub>O<sub>2</sub>/pyridine generating system.** 100 mM CalixMPO in pyridine (10  $\mu$ L) was diluted with 35  $\mu$ L of pyridine. To the resulting CalixMPO pyridine solution was added aqueous 30% H<sub>2</sub>O<sub>2</sub> (5  $\mu$ L). iv)  **$\alpha$ -Hydroxyl ethyl radical.** 100 mM CalixMPO in EtOH (7.5  $\mu$ L) was diluted with EtOH (17.5  $\mu$ L) and PBS (22  $\mu$ L). To the resulting CalixMPO aqueous ethanolic solution were added 15% H<sub>2</sub>O<sub>2</sub> in PBS (2  $\mu$ L) and 90 mM FeSO<sub>4</sub> in PBS (2  $\mu$ L). v) **Hydroxyl radical.** 10 mM CalixMPO in acetonitrile (7.5  $\mu$ L) was diluted with acetonitrile (17.5  $\mu$ L) and PBS (21  $\mu$ L). To the resulting CalixMPO solution were added 15% H<sub>2</sub>O<sub>2</sub> in PBS (2  $\mu$ L) and 90 mM FeSO<sub>4</sub> in PBS (2  $\mu$ L).

#### Stopped-Flow Kinetics

- a) **UV-vis technique.** The relative rate constants of O<sub>2</sub><sup>•-</sup> addition to spin traps were measured using competitive stopped-flow technique as described in our previous studies.<sup>59</sup> KO<sub>2</sub> was used as O<sub>2</sub><sup>•-</sup> source and phenol red (PR) as competitor. The growth of the transient absorption at 575 nm from the reaction between O<sub>2</sub><sup>•-</sup> and phenol red was monitored using UV-vis spectroscopy. The plot was linear during the first 5–8 s. The data were fitted to a

linear equation ( $t = \nu x + c$ ), where  $\nu$  is initial rate of product formation in the presence of various concentrations of spin traps (ST). The resulting initial rates were applied to the following equation:  $V/\nu - 1 = (k_{ST}[ST])/(k_{PR}[PR])$ , where  $V$  is the initial rate of formation in the absence of spin traps;  $k_{ST}$  and  $k_{PR}$  were rate constants of  $O_2^{\bullet-}$  reaction with spin trap and phenol red, respectively, while [ST] and [PR] are the concentrations of spin trap and phenol red (500  $\mu$ M), respectively. According to the plots of  $V/\nu - 1$  versus  $[ST]/[PR]$ , the values of  $k_{CalixMPO}/k_{PR}$ ,  $k_{Calix-OEt}/k_{PR}$  and  $k_{DMPO}/k_{PR}$  were determined to  $12.0 \pm 1.5$ ,  $2.0 \pm 0.3$  and  $0.03 \pm 0.00$ , respectively. **b) EPR technique.** An AquaX multiple-capillaries EPR cell was used for this experiment in which the cell was connected by a 20 gauge regular wall PTFE tube to a mixer that is also connected to two separate 1 mL syringe compartments. The cell was purged with ~ 2 mL DMSO. For all the experiments, the total reaction volume was 1 mL in which one syringe contains 0.5 mL solution of the nitrone and another syringe contains 0.5 mL solution composed of 250  $\mu$ L  $KO_2$  saturated DMSO and diluted with 250  $\mu$ L DMSO. Nitrone concentrations used were (in mM): 0.02, 0.5, 1.0, 5 and 10. Due to the limited quantity of CalixMPO, only the 3 lowest concentrations were used for comparison with other nitrones. The two solutions were injected simultaneously after one complete blank scan.

### EPR Decay Kinetics

The  $KO_2$  generating system as  $O_2^{\bullet-}$  source was used. A 100 mM CalixMPO solution in DMSO (7.5  $\mu$ L) was diluted with PBS (7.5  $\mu$ L) and DMSO (30  $\mu$ L). Superoxide adduct was generated by adding saturated  $KO_2$  solution in DMSO (5  $\mu$ L) to the resulting CalixMPO solution (45  $\mu$ L). The solution was transferred to 50  $\mu$ L capillary tube and incremental scan of the EPR spectra was obtained.

### Kinetic Analysis of EPR Spectra

Analysis of the EPR spectra was carried out by an automatic fitting program.<sup>73</sup> The half-life ( $t_{1/2}$ ) of the adducts was measured by fitting an exponential curve  $\exp(-\log 2 \times t/t_{1/2})$  on the concentration data from the decay kinetics. For the rate constants of trapping, the EPR measurements only allowed to give a crude estimation, which offered a trend for the scavenging efficiency of different nitrones. We investigated from a series of nitrone concentrations the lowest concentration where EPR signal can be detected after spin trapping. These concentrations were found to be 0.5 mM for CalixMPO, EMPO and AMPO, and 1.0 mM for DMPO and DEPMPO. At these minimal concentrations, the rate of trapping is slow compared to the dismutation of  $O_2^{\bullet-}$  and thus the build-up rate is proportional to the rate constant of scavenging.

## Conclusions

Computational studies showed that both  $O_2^{\bullet-}$  and  $HO_2^{\bullet}$  have higher affinity to calix[4]pyrrole compared to other anions and neutral substrates. Complexation of  $HO_2^{\bullet}$  and  $HO^{\bullet}$  to the calix[4]pyrrole resulted in the formation of  $HO_2^-$  and  $HO^-$ , respectively, and [calix[4]pyrrole] $^{*+}$ . However, complexation of  $O_2^{\bullet-}$  with calix[4]pyrrole did not result in redox reaction but polarization of the electronic properties of  $O_2^{\bullet-}$  was evident. The addition of  $O_2^{\bullet-}$  to nitrone was thermodynamically and kinetically more favorable when the calix[4]pyrrole was conjugated to the nitrone than when there was no conjugation. The thermodynamics of  $O_2^{\bullet-}$  complexation to calix[4]pyrrole and its addition to CalixMPO in the presence of  $Na^+$  counter-cation was also explored, and results indicate that the H-bond interaction of  $O_2^{\bullet-}$  with the calix[4]pyrrole moiety is more preferred than subsequent inclusion of  $Na^+$ . Pendant-type conjugation of the nitrone to calix[4]pyrrole was found to be the most efficient design for  $O_2^{\bullet-}$  trapping. <sup>1</sup>H NMR studies showed that the nitronyl-H chemical shift was solvent dependent due to the conformational changes on the

calix[4]pyrrole suggesting shielding effect by the pyrrole moiety. Moreover, H-bond interaction of the calix[4]pyrrole-NH's with the nitronyl-oxygen increased the charge density on the nitronyl-carbon, the site of radical addition. The  $O_2^{\bullet-}$  addition to CalixMPO was exoergic compared to the endoergic reactivity of  $O_2^{\bullet-}$  with AMPO, DMPO, EMPO and DEPMPO while the energy barrier for  $O_2^{\bullet-}$  to CalixMPO was comparable to that of AMPO. The  $HO_2^{\bullet}$  addition to CalixMPO was comparable to those of EMPO but more exoergic than AMPO, DEPMPO, and DMPO indicating that the nature of  $HO_2^{\bullet}$  addition to CalixMPO was electrophilic, and that electrostatics and H-bonding played a minor role in the favorability of  $HO_2^{\bullet}$  addition to CalixMPO.

Spin trapping using various radical generating systems yielded  $O_2^{\bullet-}$ ,  $CH_3^{\bullet}CHOH$ , and  $HO^{\bullet}$  adducts, and gave distinctive EPR spectra. Using UV-vis competitive stopped-flow kinetics in  $DMF/H_2O$ , the rate constant for the formation of CalixMPO- $O_2^{\bullet-}$  adduct was approximated to be  $k_2 \sim 680 M^{-1}s^{-1}$  which is the highest rate constant observed so far for a nitrones at the experimental conditions used in this work. The high reactivity of  $O_2^{\bullet-}$  was rationalized to be due to a synergistic effect from the polarization of  $O_2^{\bullet-}$  through H-bonding with calix[4]pyrrole, enhanced positivity of the nitronyl-C, and proximity of the nitrone group to the calix[4]pyrrole via conjugation. The half-life of the spin adduct was determined to be  $t_{1/2} = 25$  min in DMSO compared to DMPO- $O_2^{\bullet-}$  adduct with  $t_{1/2} = 6.1$  min. The high rate constant and long half-life of the CalixMPO- $O_2^{\bullet-}$  formation and decay, respectively, were further independently confirmed by using EPR stopped flow technique in pure DMSO, and follows the trend observed using UV-vis competitive stopped-flow method. Since the solubility of CalixMPO in water was limited, design and synthesis of calix[4]pyrrole that is co-conjugated with solubilizing ligands is now being addressed. This study calls for future design of spin traps and other probes that incorporates functional anion receptors to be an efficient trap for  $O_2^{\bullet-}$ . This application of anion receptors can pave the way for a more robust detection of reactive oxygen and nitrogen species and can lead to better understanding of the most important radical-mediated mechanisms in chemical and biological systems.

## Supplementary Material

Refer to Web version on PubMed Central for supplementary material.

## Acknowledgments

This publication was made possible by grant number RO1 HL81248 from the NIH National Heart, Lung, and Blood Institute. This work was supported in part by an allocation of computing time from the Ohio Supercomputer Center.

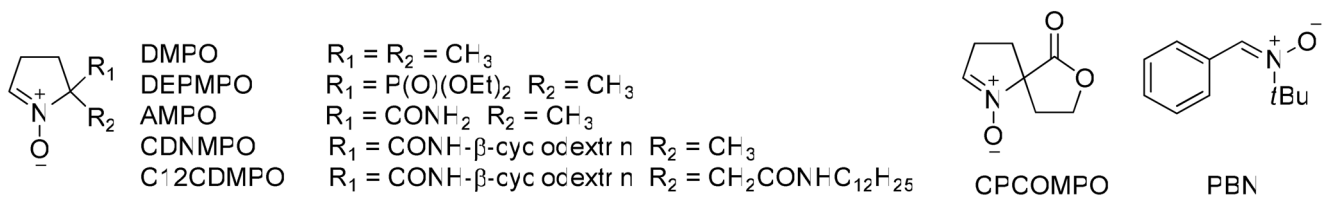
## References

1. Afanas'ev, IB. Superoxide Ion: Chemistry and Biological Implications. Vol. 1. CRC Press; Boca Raton, FL: 1989. Afanas'ev, IB. Superoxide Ion: Chemistry and Biological Implications. Vol. 2. CRC Press; Boca Raton, FL: 1991. Pickering KD, Wiesner MR. Environ Sci Tech. 2005; 39:1359–1365.
2. Crisostomo AG, Moreno RB, Navaratnam S, Wilkinson JA, Bisby RH. Free Radical Res. 2007; 41:730–737. [PubMed: 17516246] Garg S, Rose AL, Waite TD. Photochem Photobiol. 2007; 83:904–913. [PubMed: 17645662] Yamakoshi Y, Sueyoshi S, Fukuhara K, Miyata N, Masumizu T, Kohno M. J Am Chem Soc. 1998; 120:12363–12364.
3. Lambeth JD. Nat Rev Immunol. 2004; 4:181–189. [PubMed: 15039755]
4. Lambert AJ, Brand MD. Methods Mol Biol. 2009; 554:165–181. [PubMed: 19513674]
5. Nishino T, Okamoto K, Eger BT, Pai EF, Nishino T. FEBS Journal. 2008; 275:3278–3289. [PubMed: 18513323]

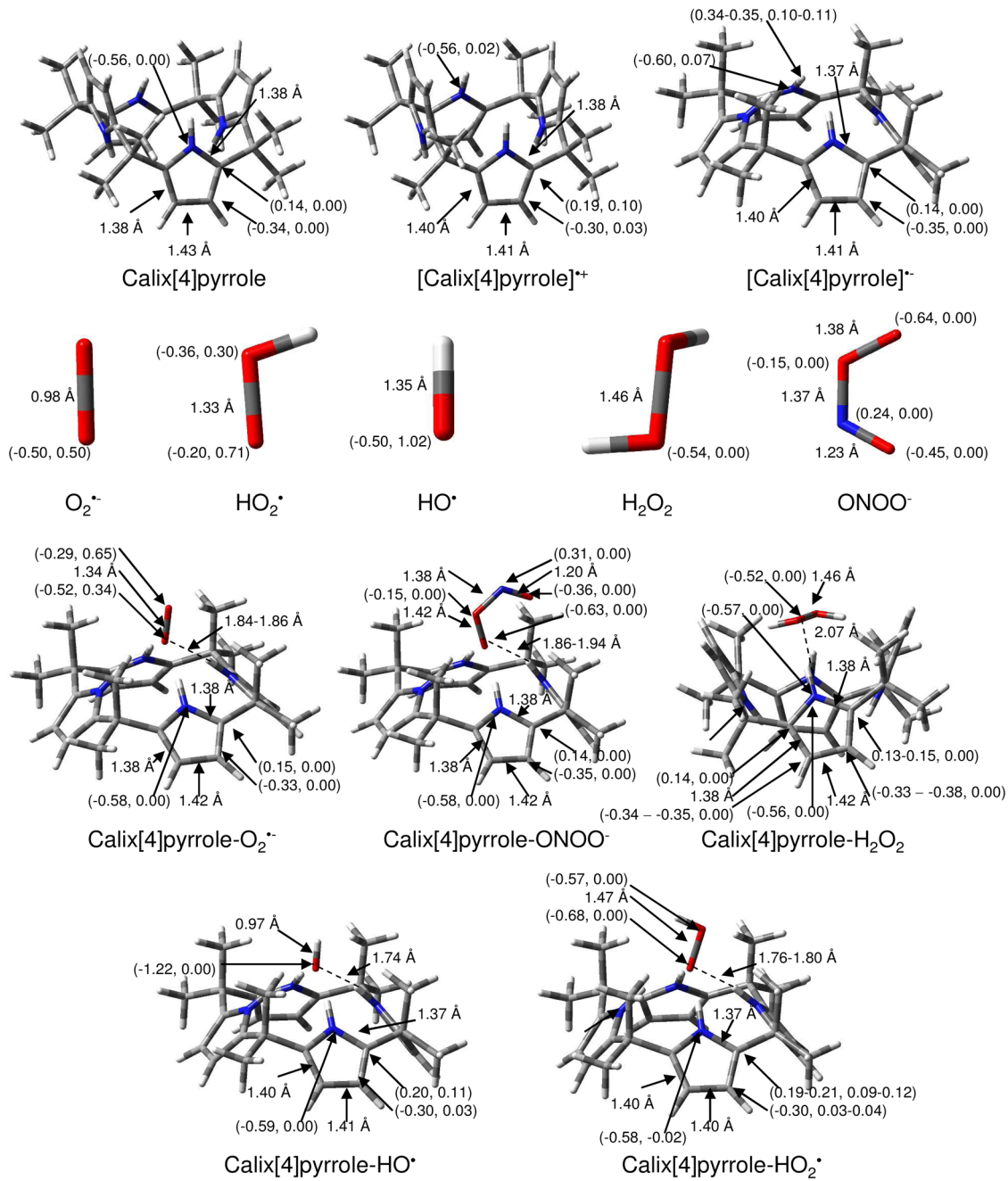
6. Xia Y, Dawson VL, Dawson TM, Synder SH, Zweier JL. Proc Natl Acad Sci U S A. 1996; 93:6770–6774. [PubMed: 8692893]
7. Gutierrez J, Ballinger SW, Darley-Usmar VM, Landar A. Circ Res. 2006; 99:924–932. [PubMed: 17068300]
8. Dreher D, Junod AF. Eur J Cancer, Part A. 1996; 32A:30–38.
9. Petrone WF, English DK, Wong K, McCord JM. Proc Natl Acad Sci U S A. 1980; 77:1159–1163. [PubMed: 6928666]
10. Floyd RA. Aging Cell. 2006; 5:51–57. [PubMed: 16441843]
11. Finkel T, Holbrook NJ. Nature. 2000; 408:239–247. [PubMed: 11089981] Zweier JL, Talukder MAH. Cardiovasc Res. 2006; 70:181–190. [PubMed: 16580655]
12. Zareba M, Szewczyk G, Sarna T, Hong L, Simon JD, Henry MM, Burke JM. Photochem Photobiol. 2006; 82:1024–1029. [PubMed: 17205626]
13. Chen YR, Chen CL, Yeh A, Liu X, Zweier JL. J Biol Chem. 2006; 281:13159–13168. [PubMed: 16531408] Dugan LL, Sensi SL, Canzoniero LMT, Handran SD, Rothman SM, Lin TS, Goldberg MP, Choi DW. J Neurosci. 1995; 15:6377–6388. [PubMed: 7472402]
14. Pospisil P, Arato A, Krieger-Liszakay A, Rutherford AW. Biochemistry. 2004; 43:6783–6792. [PubMed: 15157112] Rahimipour S, Palivan C, Barbosa F, Bilkis I, Koch Y, Weiner L, Fridkin M, Mazur Y, Gescheidt G. J Am Chem Soc. 2003; 125:1376–1384. [PubMed: 12553841]
15. Xia Y, Roman LJ, Masters BSS, Zweier JL. J Biol Chem. 1998; 273:22635–22639. [PubMed: 9712892] Xia Y, Tsai AL, Berka V, Zweier JL. J Biol Chem. 1998; 273:25804–25808. [PubMed: 9748253]
16. Serrano CV Jr, Mikhail EA, Wang P, Noble B, Kuppusamy P, Zweier JL. Biochim Biophys Acta, Mol Basis Dis. 1996; 1316:191–202. Varadharaj S, Watkins T, Cardounel AJ, Garcia JGN, Zweier JL, Kuppusamy P, Natarajan V, Parinandi NL. Antioxid Redox Signaling. 2005; 7:287–300.
17. Jackson HL, Cardounel AJ, Zweier JL, Lockwood SF. Bioorg Med Chem Lett. 2004; 14:3985–3991. [PubMed: 15225712]
18. Wang P, Chen H, Qin H, Sankarapandi S, Becher MW, Wong PC, Zweier JL. Proc Natl Acad Sci U S A. 1998; 95:4556–4560. [PubMed: 9539776]
19. Zweier JL, Flaherty JT, Weisfeldt ML. Proc Natl Acad Sci U S A. 1987; 84:1404–1407. [PubMed: 3029779] Zweier JL, Kuppusamy P, Lutty GA. Proc Natl Acad Sci U S A. 1988; 85:4046–4050. [PubMed: 2836868] Zweier JL, Kuppusamy P, Williams R, Rayburn BK, Smith D, Weisfeldt ML, Flaherty JT. J Biol Chem. 1989; 264:18890–18895. [PubMed: 2553726]
20. Bosnjakovic A, Kadirov MK, Schlick S. Res Chem Intermed. 2007; 33:677–687. Bosnjakovic A, Schlick S. J Phys Chem B. 2006; 110:10720–10728. [PubMed: 16771319] Danilczuk M, Bosnjakovic A, Kadirov MK, Schlick S. J Power Sources. 2007; 172:78–82.
21. Babu S, Velez A, Wozniak K, Szydlowska J, Seal S. Chem Phys Lett. 2007; 442:405–408. Ionita P, Conte M, Gilbert BC, Chechik V. Org Biomol Chem. 2007; 5:3504–3509. [PubMed: 17943210] Kagan VE, Tyurina YY, Tyurin VA, Konduru NV, Potapovich AI, Osipov AN, Kisin ER, Schwegler-Berry D, Mercer R, Castranova V, Shvedova AA. Toxicol Lett. 2006; 165:88–100. [PubMed: 16527436]
22. Fu H, Zhang L, Zhang S, Zhu Y, Zhao J. J Phys Chem B. 2006; 110:3061–3065. [PubMed: 16494309]
23. Xiao G, Wang X, Li D, Fu X. J Photochem Photobiol, A. 2008; 193:213–221. Chang Q, He H, Zhao J, Yang M, Qu J. Environ Sci Technol. 2008; 42:1699–1704. [PubMed: 18441823] Yu JC, Ho W, Yu J, Yip H, Wong PK, Zhao J. Environ Sci Technol. 2005; 39:1175–1179. [PubMed: 15773492]
24. Zeng Z, Zhou J, Zhang Y, Qiao R, Xia S, Chen J, Wang X, Zhang B. J Phys Chem B. 2007; 111:2688–2696. [PubMed: 17315917] Rajendran M, Inbaraj JJ, Gandhidasan R, Murugesan R. J Photochem Photobiol, A. 2006; 182:67–74. Mroz P, Pawlak A, Satti M, Lee H, Wharton T, Gali H, Sarna T, Hamblin MR. Free Radic Biol Med. 2007; 43:711–719. [PubMed: 17664135]
25. Finkelstein E, Rosen GM, Rauckman EJ. J Am Chem Soc. 1980; 102:4994–4999.
26. Frejaville C, Karoui H, Tuccio B, le Moigne F, Culcasí M, Pietri S, Lauricella R, Tordo P. J Chem Soc, Chem Commun. 1994;1793–1794.

27. Khan N, Wilmot CM, Rosen GM, Demidenko E, Sun J, Joseph J, O'Hara J, Kalyanaraman B, Swartz HM. *Free Radic Biol Med*. 2003; 34:1473–1481. [PubMed: 12757857]
28. Iwamura M, Inamoto N. *Bull Chem Soc Jpn*. 1967; 40:703.
29. Clement JL, Tordo P. *Electron Paramagn Reson*. 2007;29–49.
30. Villamena FA, Zweier JL. *Antioxid Redox Signaling*. 2004; 6:619–629.
31. Villamena FA, Xia S, Merle JK, Lauricella R, Tuccio B, Hadad CM, Zweier JL. *J Am Chem Soc*. 2007; 129:8177–8191. [PubMed: 17564447]
32. Field SM, Villamena FA. *Chem Res Toxicol*. 2008; 21:1923–1932. [PubMed: 18816073]
33. Villamena FA, Rockenbauer A, Gallucci J, Velayutham M, Hadad CM, Zweier JL. *J Org Chem*. 2004; 69:7994–8004. [PubMed: 15527282]
34. Han Y, Liu Y, Rockenbauer A, Zweier JL, Durand G, Villamena FA. *J Org Chem*. 2009; 74:5369–5380. [PubMed: 19530689]
35. Han Y, Tuccio B, Lauricella R, Villamena FA. *J Org Chem*. 2008; 73:7108–7117. [PubMed: 18707169]
36. Winterbourn CC, Parsons-Mair HN, Gebicki S, Gebicki JM, Davies MJ. *Biochem J*. 2004; 381:241–248. [PubMed: 15025556]
37. Hardy M, Bardelang D, Karoui H, Rockenbauer A, Finet JP, Jicsinszky L, Rosas R, Ouari O, Tordo P. *Chem Eur J*. 2009; 15:11114–11118. [PubMed: 19760720]
38. Allen WE, Gale PA, Brown CT, Lynch VM, Sessler JL. *J Am Chem Soc*. 1996; 118:12471–12472. Gale PA, Anzenbacher P Jr, Sessler JL. *Coord Chem Rev*. 2001; 222:57–102. Gale PA, Sessler JL, Kral V, Lynch V. *J Am Chem Soc*. 1996; 118:5140–5141.
39. Gale PA, Sessler JL, Kral V. *Chem Commun*. 1998;1–8.
40. Aydogan A, Sessler JL, Akar A, Lynch V. *Supramol Chem*. 2008; 20:11–21.
41. Anzenbacher P Jr, Try AC, Miyaji H, Jursikova K, Lynch VM, Marquez M, Sessler JL. *J Am Chem Soc*. 2000; 122:10268–10272.
42. Anzenbacher P Jr, Jursikova K, Shriver JA, Miyaji H, Lynch VM, Sessler JL, Gale PA. *J Org Chem*. 2000; 65:7641–7645. [PubMed: 11076627]
43. Nishiyabu R, Anzenbacher P Jr. *J Am Chem Soc*. 2005; 127:8270–8271. [PubMed: 15941245]
44. Panda PK, Lee C-H. *Org Lett*. 2004; 6:671–674. [PubMed: 14986946]
45. Sessler JL, Kral V, Shishkanova TV, Gale PA. *Proc Natl Acad Sci U S A*. 2002; 99:4848–4853. [PubMed: 11929967]
46. Bucher C, Zimmerman RS, Lynch V, Kral V, Sessler JL. *J Am Chem Soc*. 2001; 123:2099–2100. [PubMed: 11456850]
47. Anzenbacher P, Nishiyabu R, Palacios MA. *Coord Chem Rev*. 2006; 250:2929–2938.
48. Akar A, Aydogan A. *J Heterocycl Chem*. 2005; 42:931–934.
49. Miyaji H, Anzenbacher P Jr, Sessler JL, Bleasdale ER, Gale PA. *Chem Commun*. 1999;1723–1724. Nielsen KA, Cho W-S, Jeppesen JO, Lynch VM, Becher J, Sessler JL. *J Am Chem Soc*. 2004; 126:16296–16297. [PubMed: 15600311]
50. Behar D, Czapski G, Rabani J, Dorfman LM, Schwarz HA. *J Phys Chem*. 1970; 74:3209–3213.
51. Allouch A, Lauricella RP, Tuccio BN. *Mol Phys*. 2007; 105:2017–2024.
52. McCormick ML, Gaut JP, Lin T-S, Britigan BE, Buettner GR, Heinecke JW. *J Biol Chem*. 1998; 273:32030–32037. [PubMed: 9822676]
53. Buettner GR. *Arch Biochem Biophys*. 1993; 300:535–543. [PubMed: 8434935]
54. Tabba HD, Cavaleiro JAS, Jeyakumar D, Graca M, Neves PMS, Smith KM. *J Org Chem*. 1989; 54:1943–1948. Cuesta L, Gross D, Lynch VM, Ou Z, Kajonkijya W, Ohkubo K, Fukuzumi S, Kadish KM, Sessler JL. *J Am Chem Soc*. 2007; 129:11696–11697. [PubMed: 17760448]
55. Custelcean R, Delmau LH, Moyer BA, Sessler JL, Cho W-S, Gross D, Bates GW, Brooks SJ, Light ME, Gale PA. *Angew Chem, Int Ed*. 2005; 44:2537–2542.
56. Nishiyabu R, Palacios MA, Dehaen W, Anzenbacher P Jr. *J Am Chem Soc*. 2006; 128:11496–11504. [PubMed: 16939273]
57. Aydogan A, Coady DJ, Kim SK, Akar A, Bielawski CW, Marquez M, Sessler JL. *Angew Chem, Int Ed*. 2008; 47:9648–9652.

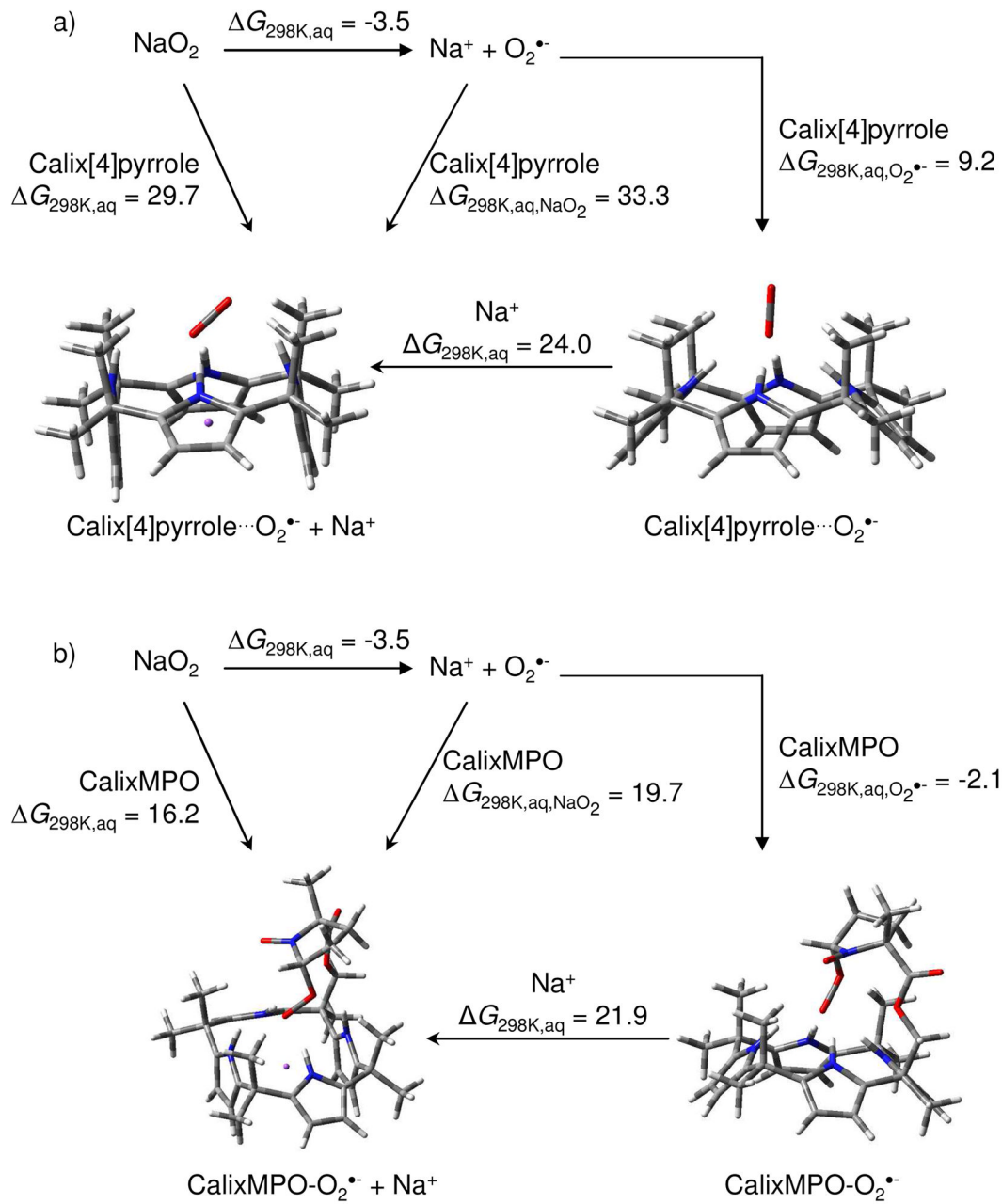
58. Villamena FA, Merle JK, Hadad CM, Zweier JL. *J Phys Chem A*. 2005; 109:6083–6088. [PubMed: 16833945]
59. Durand G, Choteau F, Pucci B, Villamena FA. *J Phys Chem A*. 2008; 112:12498–12509. [PubMed: 18998656]
60. Villamena FA, Merle JK, Hadad CM, Zweier JL. *J Phys Chem A*. 2007; 111:9995–10001. [PubMed: 17845014]
61. Aydogan A, Coady DJ, Lynch VM, Akar A, Marquez M, Bielawski CW, Sessler JL. *Chem Commun*. 2008;1455–1457.
62. Stolze K, Rohr-Udilova N, Hofinger A, Rosenau T. *Bioorg Med Chem*. 2008; 16:8082–8089. [PubMed: 18706818]
63. Bias JR, Lopez-Bes JM, Mirquez M, Sessler JL, Javier F, Orozco M. *Chem-Eur J*. 2007; 13:1108–1116. [PubMed: 17086569]
64. Burgett RA, Bao X, Villamena FA. *J Phys Chem A*. 2008; 112:2447–2455. [PubMed: 18303874]
65. Han Y, Tuccio B, Lauricella R, Rockenbauer A, Zweier JL, Villamena FA. *J Org Chem*. 2008; 73:2533–2541. [PubMed: 18331054]
66. Villamena FA. *J Phys Chem A*. 2010; 114:1153–1160. [PubMed: 19968309]
67. Villamena FA. *J Phys Chem A*. 2009; 113:6398–6403. [PubMed: 19425559]
68. Labanowski, JW.; Andzelm, J. *Density Functional Methods in Chemistry*. Springer; New York: 1991.
69. Frisch, MJ., et al. Gaussian, Inc. Wallingford, CT: 2004.
70. Villamena FA, Liu Y, Zweier JL. *J Phys Chem A*. 2008; 112:12607–12615. [PubMed: 19012384]
71. Scott AP, Radom L. *J Phys Chem*. 1996; 100:16502–16513.
72. Reed AE, Curtiss LA, Weinhold F. *Chem Rev*. 1988; 88:899–926.
73. Rockenbauer A, Korecz L. *Appl Magn Reson*. 1996; 10:29–43.



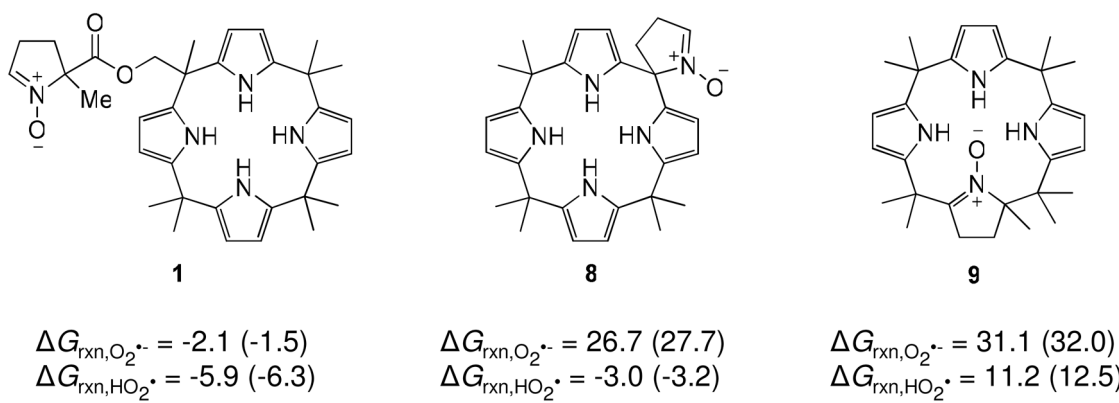
**Figure 1.**  
Structures of cyclic nitroxyl spin traps

**Figure 2.**

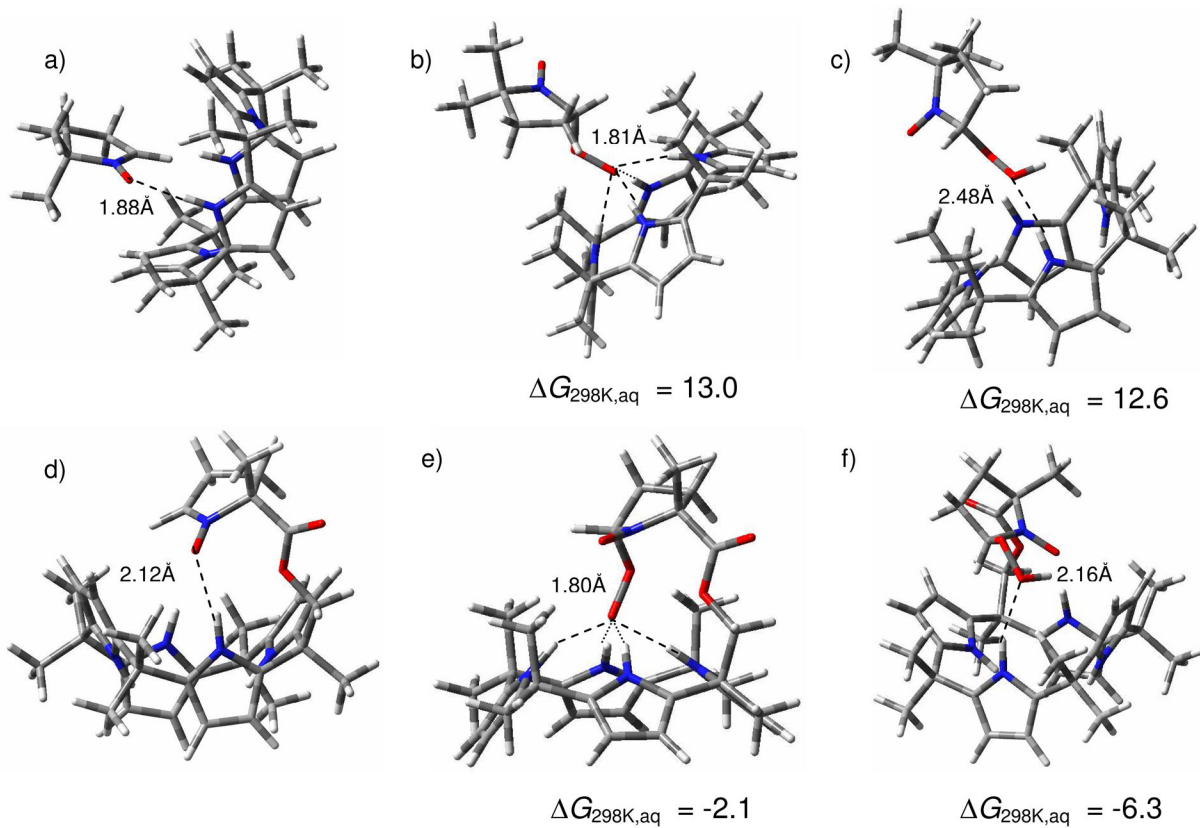
Optimized structures for calix[4]pyrrole complexes including charge (left) and spin (right) densities (in parentheses), and bond lengths (in Å) at the PCM(water)/B3LYP/6-31+G(d,p)//B3LYP/6-31G(d) level of theory: First row: octamethyl calix[4]pyrrole and its radical cation and anion; Second row: O<sub>2</sub><sup>•-</sup>, HO<sub>2</sub><sup>•</sup>, HO<sup>•</sup>, H<sub>2</sub>O<sub>2</sub>, and ONOO<sup>-</sup>; Third row: *meso*-octamethyl calix[4]pyrrole complexes with O<sub>2</sub><sup>•-</sup>, ONOO<sup>-</sup>, and H<sub>2</sub>O<sub>2</sub>; Fourth row: *meso*-octamethyl calix[4]pyrrole complexes with HO<sup>•</sup> and HO<sub>2</sub><sup>•</sup>.

**Figure 3.**

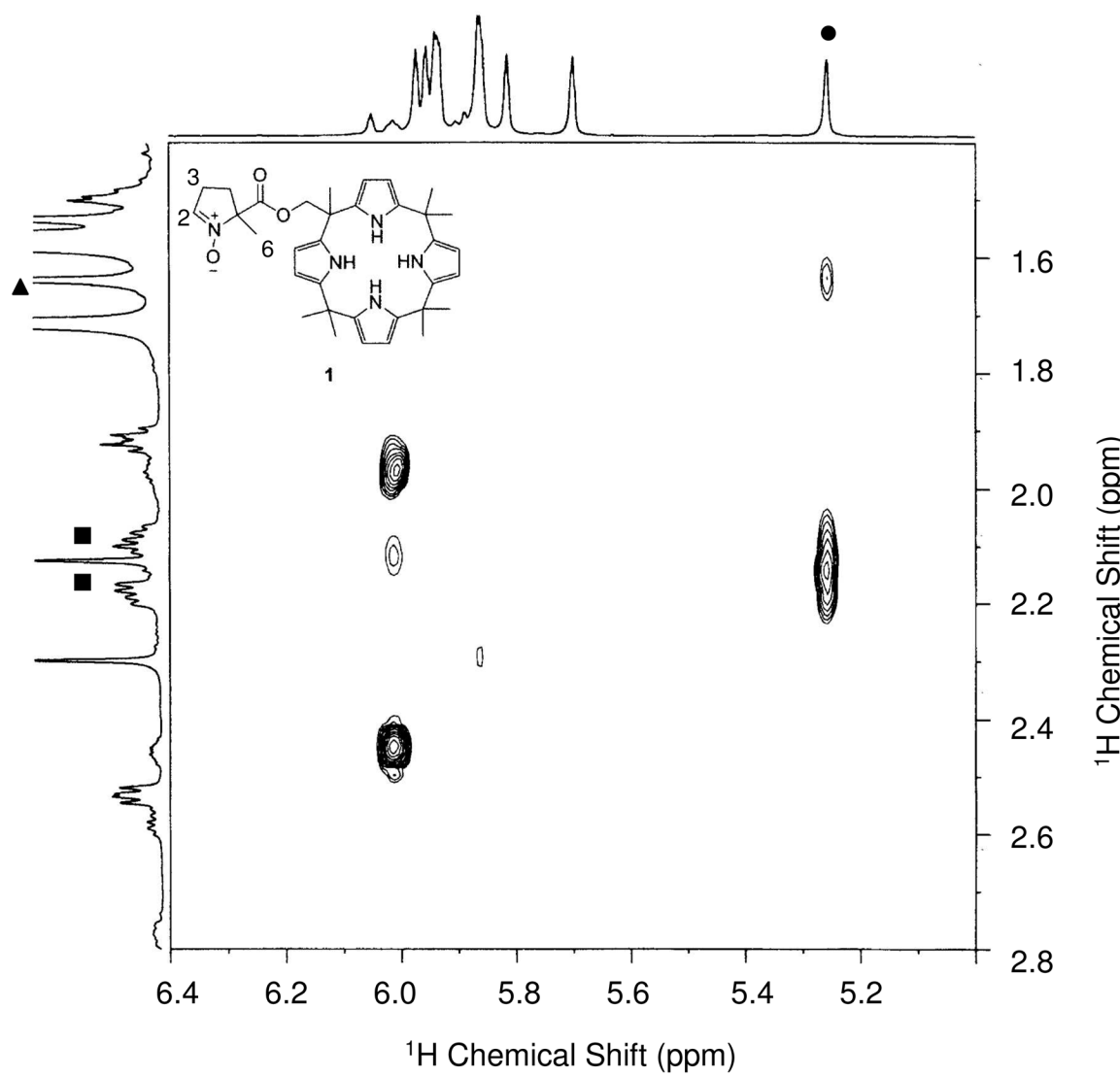
Calculated free energies (in kcal/mol) for complex formations of a) *meso*-octamethyl calix[4]pyrrole and b) CalixMPO- $\text{O}_2^{\bullet-}$  adduct with sodium counterion (in purple) in aqueous phase at the PCM/B3LYP/6-31+G(d,p)//B3LYP/6-31G(d) level of theory

**Figure 4.**

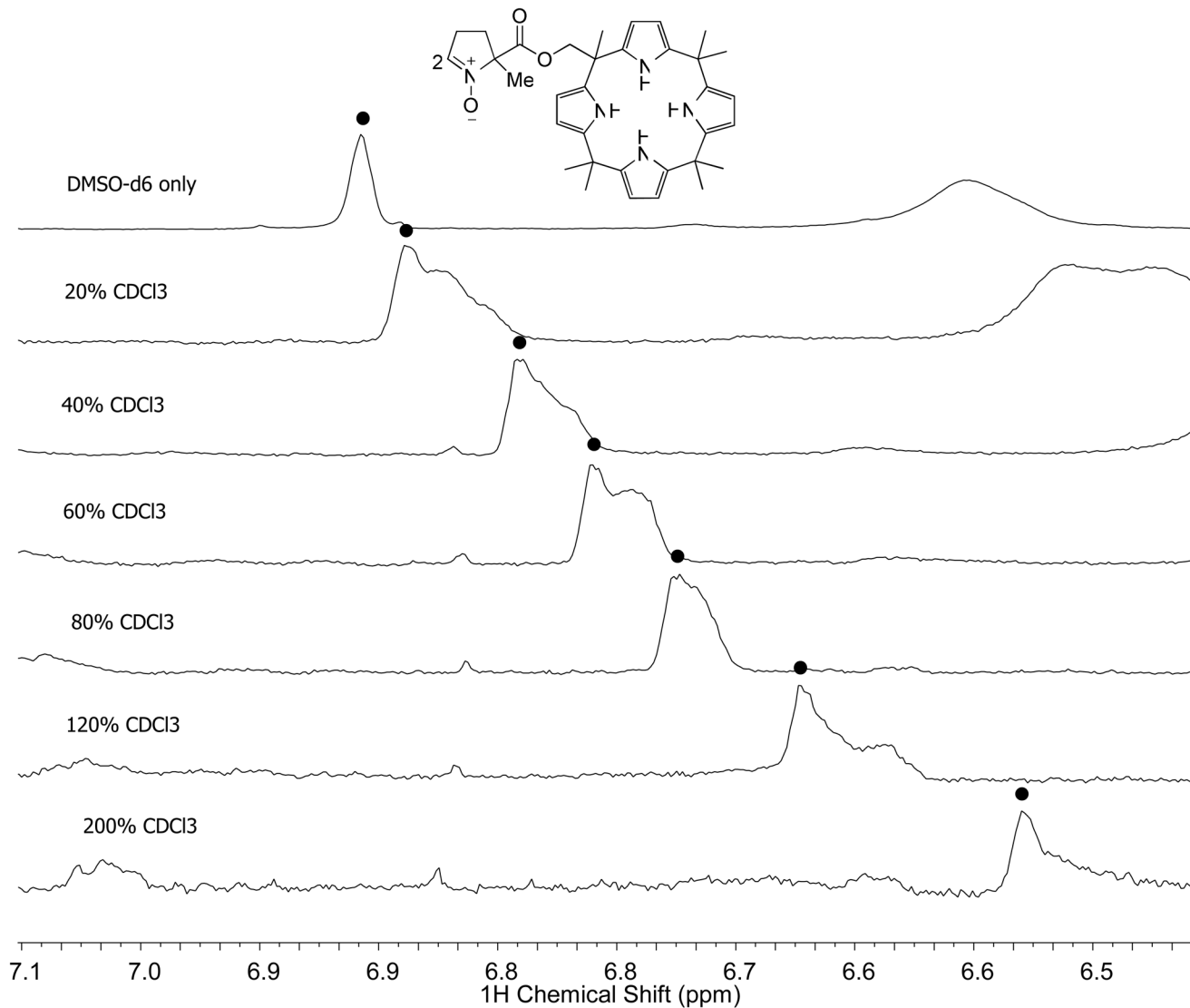
Designs of calix[4]pyrrole-containing nitrone spin traps, and their calculated free energies of reaction with  $O_2^{\cdot-}$  and  $HO_2^{\cdot}$  ( $\Delta G_{298K,aq}$  in kcal/mol) in aqueous phases and DMSO (in parentheses).

**Figure 5.**

Lowest energy conformations in aqueous phase of a) *meso*-octamethyl calix[4]pyrrole + DMPO complex; b) *meso*-octamethyl calix[4]pyrrole + DMPO-O<sub>2</sub><sup>•-</sup> adduct; c) *meso*-octamethyl calix[4]pyrrole + DMPO-O<sub>2</sub>H adduct; d) CalixMPO; e) CalixMPO-O<sub>2</sub><sup>•-</sup> adduct; f) CalixMPO-O<sub>2</sub>H adduct with reaction free energies ( $\Delta G_{298K,aq}$  in kcal/mol) and bond length ranges (Å) at PCM/B3LYP/6-31+G(d,p)//B3LYP/6-31G(d) level of theory.

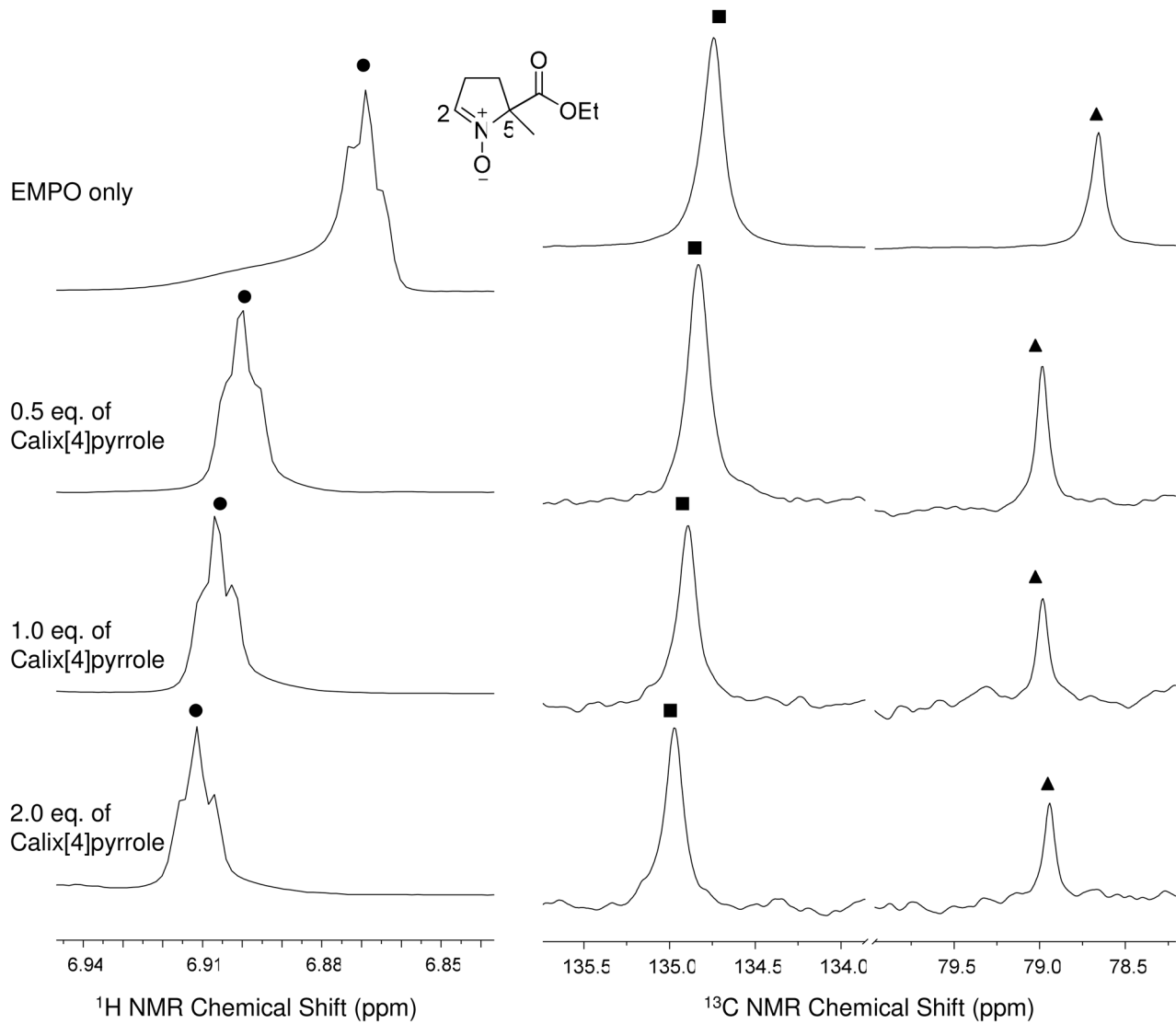
**Figure 6.**

Expanded COSY spectrum of CalixMPO in  $\text{CDCl}_3$  showing correlation of nitronyl H-2 (marked by ●) with H-3 (marked by ■) and H-6 (marked by ▲).

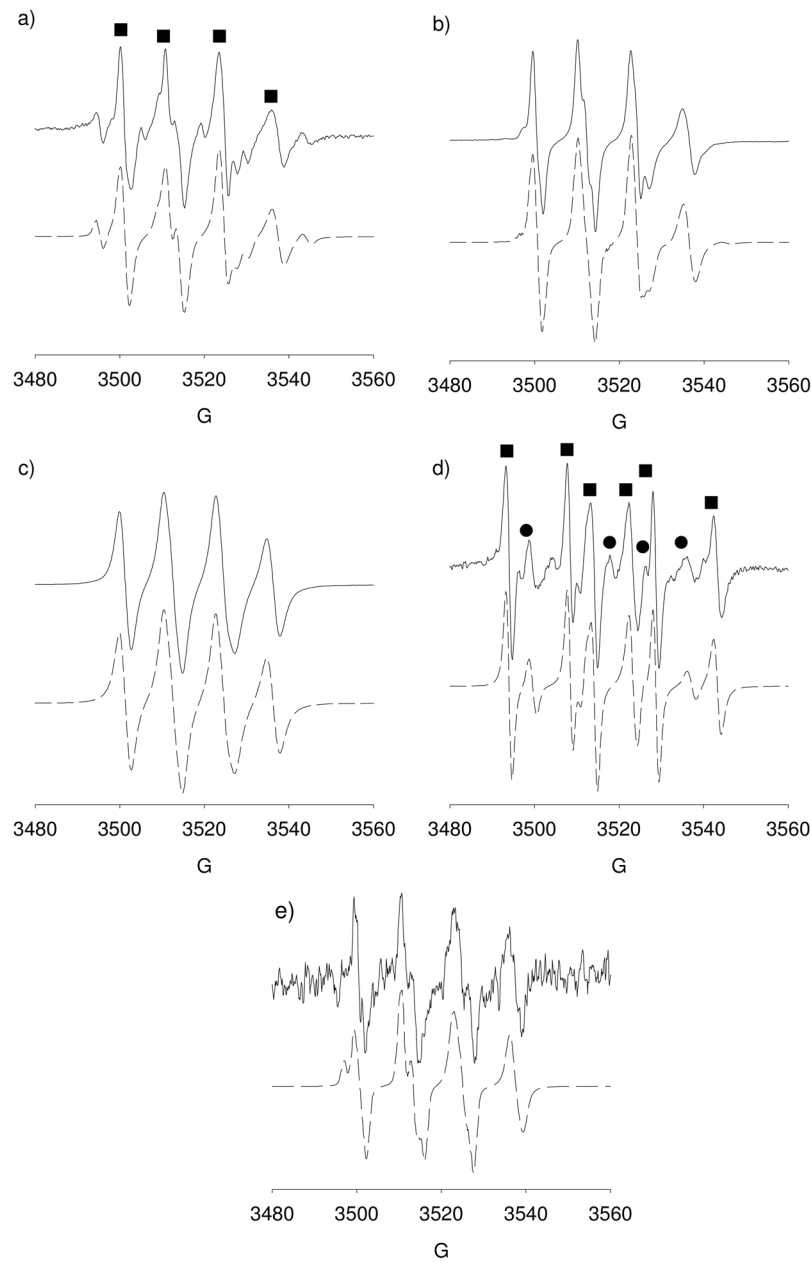


**Figure 7.**

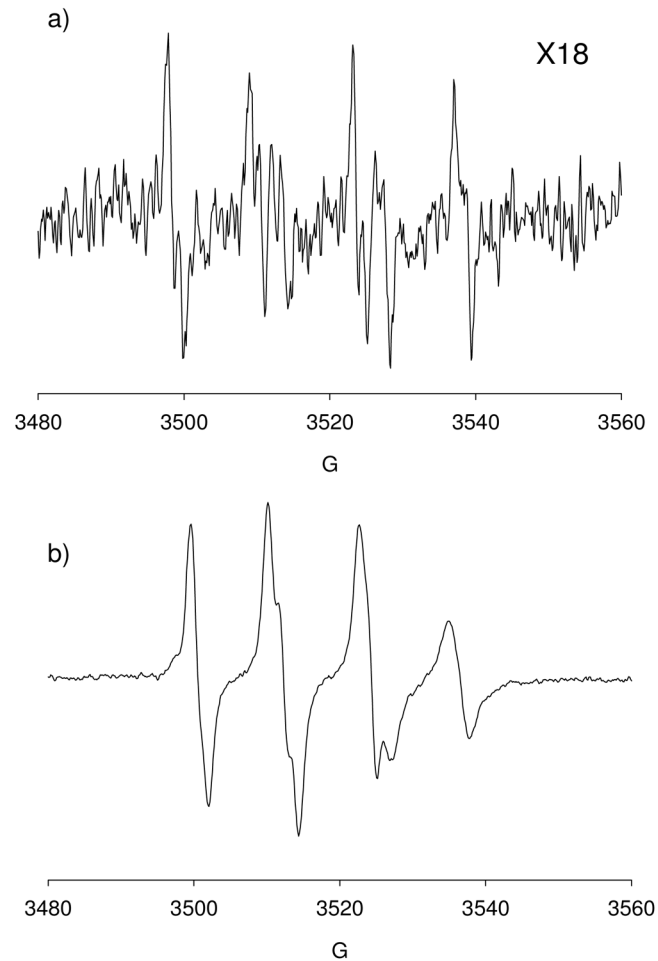
<sup>1</sup>H NMR spectra showing the upfield shift of the nitronyl H-2 (marked by ●) of CalixMPO as a function of increasing CDCl<sub>3</sub> concentrations in DMSO-*d*<sub>6</sub>.

**Figure 8.**

$^1\text{H}$  (left) and  $^{13}\text{C}$  (right) NMR spectra showing the downfield shift of the nitronyl H-2 (marked by ●), C-2 (marked by ■), and quartenary carbon (C-5, marked by ▲) of EMPO at increasing equivalents of *meso*-octamethyl calix[4]pyrrole in  $\text{CDCl}_3$ .

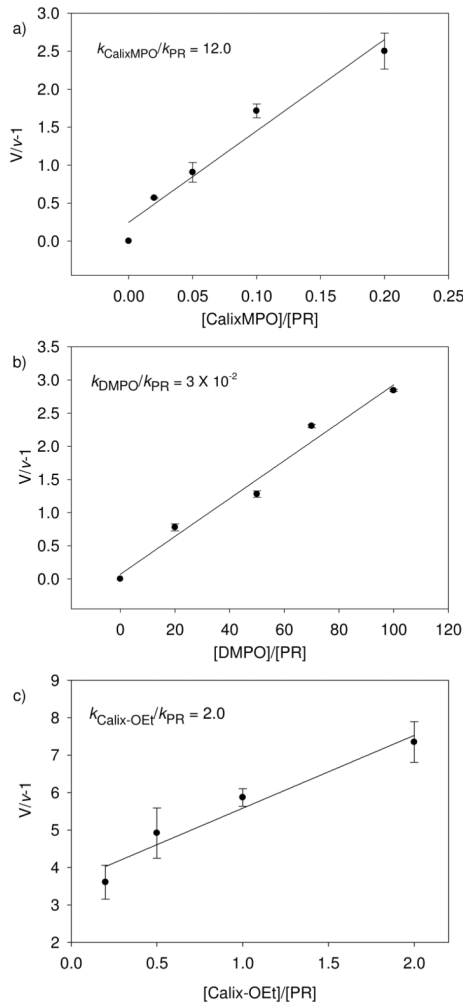
**Figure 9.**

X-band EPR spectra of superoxide adducts of CalixMPO generated from a) riboflavin/h $\nu$  in 50% CH<sub>3</sub>CN in PBS. I, 60% (marked by ■):  $a_N = 12.95$  G,  $a_H = 11.11$  G; II, 22%:  $a_N = 12.58$  G,  $a_H = 8.64$  G; alkyl adduct, 18%:  $a_N = 14.48$  G,  $a_H = 20.70$  G; b) KO<sub>2</sub> in DMSO with 15% PBS. 97%:  $g = 2.0057$ ,  $a_N = 12.64$  G,  $a_H = 10.61$  G; unknown, 3%:  $g = 2.0054$ ,  $a_N = 14.40$  G,  $a_H = 19.0$  G; c) H<sub>2</sub>O<sub>2</sub> in pyridine with 10% PBS. 100%:  $g = 2.0058$ ,  $a_N = 12.39$  G,  $a_H = 10.31$  G;  $a_{H'} = 1.13$  G; and d) CH<sub>3</sub>•CHOH adduct generated from H<sub>2</sub>O<sub>2</sub>/FeSO<sub>4</sub> in PBS with 50% EtOH. 80% (marked by ■):  $g = 2.0054$ ,  $a_N = 14.51$  G,  $a_H = 20.27$  G, and HO• adduct, 20% (marked by ●):  $g = 2.0056$ ,  $a_N = 13.38$  G,  $a_H = 10.80$  G; e) HO• adduct generated from H<sub>2</sub>O<sub>2</sub>/FeSO<sub>4</sub> in PBS with 50% acetonitrile.  $g = 2.0056$ ,  $a_N = 13.79$  G,  $a_H = 11.65$  G.

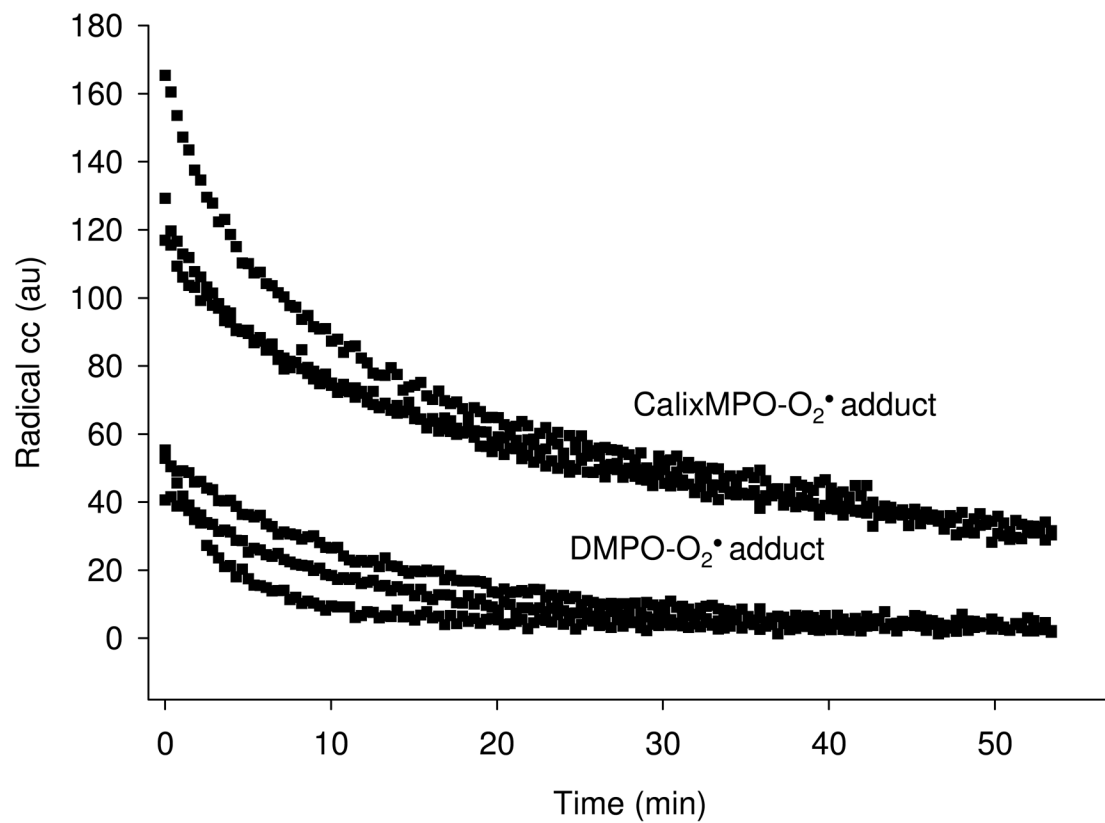


**Figure 10.**

Single scan EPR spectra of  $\text{O}_2^{\bullet-}$  adducts of DMPO (15 mM) and CalixMPO (15 mM) generated using  $\text{KO}_2$  in DMSO with 15% PBS.

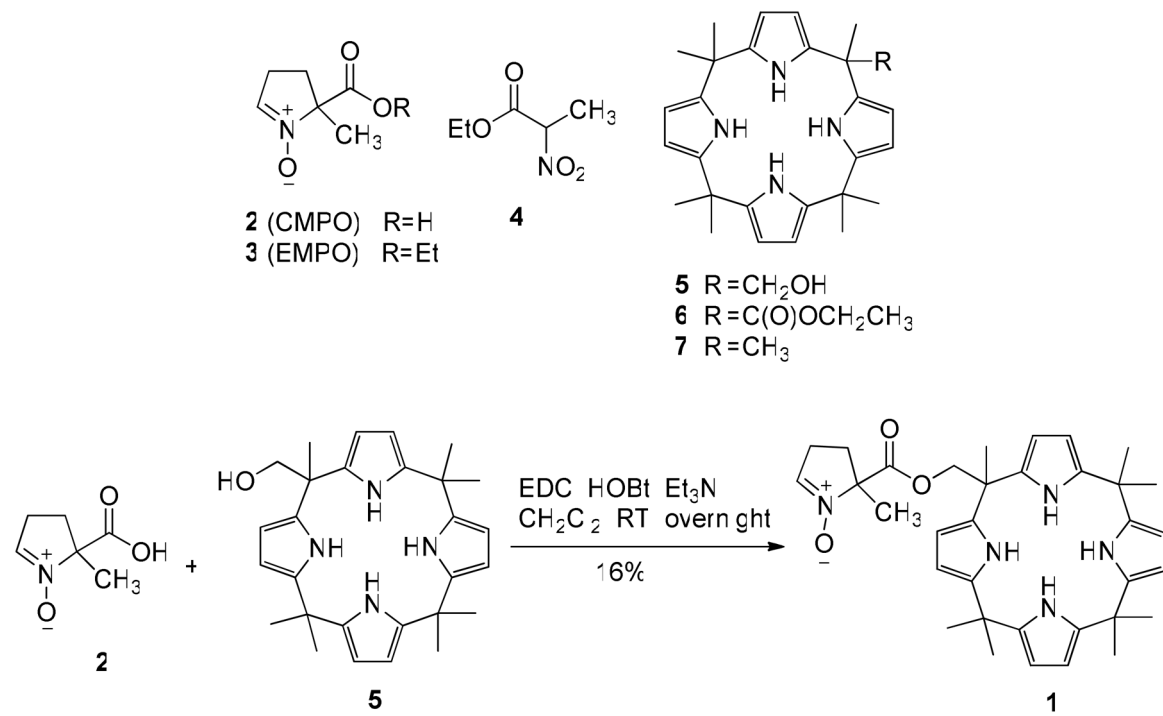
**Figure 11.**

Stopped-flow kinetic plots of a) CalixMPO-O<sub>2</sub><sup>•-</sup> adduct; b) DMPO-O<sub>2</sub><sup>•-</sup> adduct; and c) calix[4]pyrrole ethyl ester-O<sub>2</sub><sup>•-</sup> complex. Radical was generated using KO<sub>2</sub> in DMF and using phenol red (PR) as competitor, where V and  $\nu$  are the initial rates of formation in the absence and presence of various concentrations of the spin trap, respectively.



**Figure 12.**

Decay plots  $\text{O}_2^{\bullet-}$  adducts generated from CalixMPO (15 mM) and DMPO (15 mM) using  $\text{KO}_2$  in DMSO with 15% PBS. The calculated half-lives were *ca.* 25 and 6 min, for CalixMPO- $\text{O}_2\text{H}$  and DMPO- $\text{O}_2\text{H}$ , respectively.

**Scheme 1.**Synthesis of CalixMPO (**1**) and structures of intermediates (**2** through **7**)

**Table 1**

Calculated enthalpies ( $\Delta H_{298K}$ ) and free energies ( $\Delta G_{298K}$ ) in kcal/mol for complex formation of *meso*-octamethyl calix[4]pyrrole with the selected anions, neutral substrates,  $O_2^\bullet-$ ,  $HO_2^\bullet$ , and  $HO^\bullet$  in aqueous phase and DMSO (in parentheses) at the PCM/B3LYP/6-31+G(d,p)//B3LYP/6-31G(d) and PCM/B3LYP/6-311+G(d,p)//B3LYP/6-31G(d) level of theory, and bond length ranges (Å) for the pyrrole-NH···X.

X	PCM/B3LYP/6-31+G(d,p)			PCM/B3LYP/6-311+G(d,p)			NH···X
	$\Delta H_{298K}$	$\Delta G_{298K}$	$\Delta H_{298K}$	$\Delta G_{298K}$	$\Delta H_{298K}$	$\Delta G_{298K}$	
Benzolate	5.4 (2.7)	19.3 (16.6)	5.8 (3.1)	19.7 (17.0)	1.81–1.89		
Br <sup>-</sup>	-9.3 (-12.9)	2.9 (-0.8)	7.5 (3.8)	19.6 (16.0)	2.43		
Cl <sup>-</sup>	3.4 (-0.6)	14.7 (10.7)	3.0 (-0.8)	14.4 (10.5)	2.34		
CN <sup>-</sup>	1.7 (3.2)	11.9 (13.5)	2.4 (-1.5)	12.6 (8.7)	2.05–2.07		
ONOO <sup>-</sup>	-5.5 (-9.4)	8.8 (5.0)	-6.3 (-10.1)	8.0 (4.2)	1.85–1.89		
Acetone	4.3 (0.4)	16.4 (12.4)	4.4 (0.5)	16.5 (12.5)	2.00		
Methanol	4.1 (0.3)	14.8 (11.0)	4.3 (0.4)	15.0 (11.2)	1.93		
H <sub>2</sub> O <sub>2</sub>	3.15 (-1.2)	15.9 (11.6)	3.3 (-1.2)	16.0 (11.6)	2.07		
O <sub>2</sub> <sup>•-</sup>	-2.5 (-6.4)	9.2 (5.3)	-3.0 (-6.9)	8.7 (4.8)	1.84–1.87		
HO <sub>2</sub> <sup>•</sup>	-4.0 (-7.6)	9.3 (5.7)	-4.1 (-7.8)	9.2 (5.4)	1.76–1.80		
HO <sup>•</sup>	-34.5 (-38.8)	-21.6 (-25.9)	-33.8 (-38.2)	-20.9 (-25.3)	1.74		

**Table 2**

Calculated enthalpies ( $\Delta H_{298K}$ ) and free energies ( $\Delta G_{298K}$ ) in kcal/mol for  $O_2^{\bullet-}$  and  $HO_2^{\bullet}$  spin adducts formation with unconjugated calix[4]pyrrole-DMPO, CalixMPO, **9**, and **8** in aqueous phase and DMSO (in parentheses) along with H-bond length ranges (Å) for the pyrrole-NH<sup>-</sup>O at the PCM/B3LYP/6-31+G(d,p)//B3LYP/6-31G(d) level of theory

Structures	$\Delta H_{298K}$	$\Delta G_{298K}$	NH <sup>-</sup> $O_2^{\bullet-}$	NH <sup>-</sup> $O_2H$
Calix[4]pyrrole <sup>a</sup> -DMPO-O <sub>2</sub> <sup>•-</sup>				
Calix[4]pyrrole + DMPO + $O_2^{\bullet-}$	-9.3 (-11.9)	15.6 (13.0)		
Calix[4]pyrrole + DMPO- $O_2^{\bullet-}$	-11.4 (-14.9)	3.0 (-0.4)	1.81–1.86	N/A
Calix[4]pyrrole <sup>-</sup> $O_2^{\bullet-}$ + DMPO	-6.8 (-5.5)	6.4 (7.7)		
Calix[4]pyrrole <sup>a</sup> -DMPO-O <sub>2</sub> H				
Calix[4]pyrrole + DMPO + $O_2H$	-6.6 (-9.8)	15.9 (12.6)		
Calix[4]pyrrole + DMPO-O <sub>2</sub> H	10.3 (6.6)	20.6 (17.0)	N/A	2.24–2.83
Calix[4]pyrrole <sup>-</sup> $O_2H$ + DMPO	-2.6 (-2.3)	6.6 (7.0)		
CalixMPO-O <sub>2</sub> <sup>•-</sup>				
<i>cis</i> -adduct	-16.9 (-16.3)	-2.1 (-1.5)	1.80–1.88	N/A
<i>trans</i> -adduct	-10.0 (-8.8)	5.2 (6.4)	1.76–1.96	
CalixMPO-O <sub>2</sub> H				
<i>cis</i> -adduct	-13.9 (-13.6)	-1.9 (-1.6)	N/A	2.31
<i>trans</i> -adduct	-20.6 (-21.0)	-5.9 (-6.3)	2.16	
<b>9</b> - $O_2^{\bullet-}$				
<b>9</b> $O_2H$	18.6 (19.5)	31.1 (32.0)	<i>a</i>	<i>a</i>
<b>8</b> - $O_2^{\bullet-}$				
<b>8</b> $O_2H$	15.3 (16.2)	26.7 (27.7)	<i>a</i>	<i>a</i>
<b>8</b> - $O_2H$				
	-15.2 (-15.4)	-3.0 (-3.2)		

<sup>a</sup>No hydrogen bond observed.

**Table 3**

Calculated relative enthalpies ( $\Delta H_{298K}$ ) and free energies ( $\Delta G_{298K}$ ) in kcal/mol for  $O_2^{\bullet-}$  addition to unconjugated and conjugated calix[4]pyrrole nitroxyl in aqueous phase and DMSO (in parentheses) at the PCM/B3LYP/6-31+G(d,p)//B3LYP/6-31G(d) level of theory.

Structure	$\Delta H_{298K}$	$\Delta G_{298K}$	$C^{'''}O_2^{\bullet-}$	$\langle S^2 \rangle$	Imaginary frequency <sup>e</sup>
Calix[4]pyrrole- $O_2^{\bullet-}$ + DMPO	0	0	$\infty$	N/A	0
Calix[4]pyrrole- $O_2^{\bullet-}$ -DMPO	4.9 (6.0)	13.5 (14.6)	3.20	0.76	0
[Calix[4]pyrrole-DMPO- $O_2^{\bullet-}$ ] <sup>f</sup>	13.1 (14.3)	25.7 (26.9)	2.03	0.75	432 <i>i</i>
Calix[4]pyrrole-DMPO- $O_2^{\bullet-}$	-6.8 (-5.5)	6.4 (7.7)	1.41	0.75	0
CalixMPO + $O_2^{\bullet-}$ <sup>a</sup>	0	0	$\infty$	N/A	0
CalixMPO- $O_2^{\bullet-}$ <sup>b</sup>	-5.0 (-4.0)	7.1 (8.1)	3.44	0.76	0
[CalixMPO- $O_2^{\bullet-}$ ] <sup>c</sup>	2.9 (3.6)	17.5 (18.2)	2.00	0.80	422 <i>i</i>
CalixMPO- $O_2^{\bullet-}$ <sup>d</sup>	-16.9 (-16.3)	-2.1 (-1.5)	1.39	0.75	0

<sup>a</sup> At infinite separation;

<sup>b</sup> Complex;

<sup>c</sup> Transition state;

<sup>d</sup> Product;

<sup>e</sup> In units of  $\text{cm}^{-1}$

**Table 4**

Calculated charge densities (in e) of nitronyl-carbon (C-2), experimental and calculated rate constants (in M<sup>-1</sup>s<sup>-1</sup>), and reaction free energies (in kcal/mol) for O<sub>2</sub><sup>•-</sup> adducts formation in aqueous phase and DMSO (in parentheses) at PCM/B3LYP/6-31+G(d,p)//B3LYP/6-31G(d) level of theory.

Nitrones	Nitronyl-C charge density	Exptl ( <i>k</i> <sub>2</sub> ) <sup>a</sup>	Exptl ( <i>k</i> <sub>1</sub> ) <sup>b</sup>	Rate constant	
				Calcd	Δ <i>G</i> <sub>298K,rxn</sub>
CalixMPO	0.051 (0.045)	680	8	26.9 (8.5)	-2.1 (-1.5)
AMPQ <sup>31</sup>	0.060 (0.059)	130	4	38.7 (19.2)	6.1 (6.4)
EMPO <sup>31</sup>	0.040 (0.038)	105	2	6.8 × 10 <sup>-2</sup> (2.7 × 10 <sup>-2</sup> )	9.7 (10.3)
DMPQ <sup>31</sup>	0.019 (0.018)	2	1	5.9 × 10 <sup>-5</sup> (1.6 × 10 <sup>-5</sup> )	12.6 (13.8)
DERMPO <sup>31</sup>	0.043 (0.040)	1	1	1.5 × 10 <sup>-5</sup> (4.1 × 10 <sup>-6</sup> )	14.7 (15.4)
PBN <sup>59</sup>	0.009 (0.010)	1 × 10 <sup>-1</sup>	c	2.5 × 10 <sup>-10</sup> (6.3 × 10 <sup>-11</sup> )	18.3 (18.9)

<sup>a</sup>UV-vis stopped-flow technique was employed with KO<sub>2</sub> and phenol red as competitor in DMF:H<sub>2</sub>O 9:1.

<sup>b</sup>EPR stopped-flow technique was employed with KO<sub>2</sub> in DMSO.

cNot determined.